
Inexact Bregman Sparse Newton Method for Efficient Optimal Transport

Jianting Pan¹ Ji'an Li¹ Ming Yan¹

Abstract

Computing exact Optimal Transport (OT) distances for large-scale datasets is computationally prohibitive. While entropy-regularized alternatives offer speed, they sacrifice precision and frequently suffer from numerical instability in high-accuracy regimes. To address these limitations, we propose the Inexact Bregman Sparse Newton (IBSN) method, which efficiently solves the exact OT problems. Our approach utilizes a Bregman proximal point framework through a sequence of semi-dual subproblems. By solving these subproblems inexactly, we significantly reduce per-iteration complexity while maintaining a theoretical guarantee of convergence to the true optimal plan. To further accelerate the algorithm, we develop a sparse Newton-type solver for the subproblem and employ a Hessian sparsification strategy that drastically lowers memory and time costs without sacrificing accuracy. We provide rigorous theoretical guarantees for the global convergence of the algorithm. Extensive experiments demonstrate that IBSN consistently outperforms state-of-the-art methods in both computational speed and solution precision.

1. Introduction

Optimal transport (OT) has emerged as a fundamental tool for measuring the difference between probability distributions. Unlike standard metrics, OT offers a geometrically meaningful distance. This unique property has led to widespread applications across machine learning (Gordaliza et al., 2019; Oneto et al., 2020; Montesuma et al., 2024), computer vision (Bonnel & Digne, 2023; Rubner et al., 2000; Solomon et al., 2014), and statistics (Goldfeld et al., 2024; Klatt et al., 2020).

The discrete OT problem can be characterized by the fol-

¹School of Data Science, The Chinese University of Hong Kong, Shenzhen. Correspondence to: Ming Yan <yanming@cuhk.edu.cn>.

Preprint. March 17, 2026.

lowing linear programming problem:

$$\begin{aligned} \min_{X \in \mathbb{R}^{m \times n}} \langle C, X \rangle \\ \text{s.t. } X \in \Omega := \{X : X\mathbf{1}_n = \mathbf{a}, X^\top \mathbf{1}_m = \mathbf{b}, X \geq 0\}, \end{aligned} \quad (1)$$

where $C \in \mathbb{R}_+^{m \times n}$ is the cost matrix, $\mathbf{a} \in \mathbb{R}_+^m$, $\mathbf{b} \in \mathbb{R}_+^n$ are two vectors satisfying $\mathbf{1}_m^\top \mathbf{a} = \mathbf{1}_n^\top \mathbf{b} = 1$, $\mathbf{1}_m$ and $\mathbf{1}_n$ are the vectors of all ones in \mathbb{R}^m and \mathbb{R}^n respectively. While this formulation is linear, finding the solution of large-scale problems is computationally challenging. Classical solvers for the associated large-scale linear programs, such as interior-point (Nesterov & Nemirovskii, 1994) or network simplex methods (Burkard et al., 2012), scale poorly and become too expensive when applied to high-dimensional datasets.

To address the computational challenges, an entropic regularization term $\phi(X) = \sum_{i=1}^m \sum_{j=1}^n X_{ij} \log X_{ij}$ was introduced to the objective, which is known as entropy-regularized optimal transport (EOT) (Cuturi, 2013):

$$\min_{X \in \Omega} \langle C, X \rangle + \eta \phi(X), \quad (2)$$

where $\eta > 0$ is a regularization parameter. This modification yields a η -strongly convex problem on Ω that can be solved efficiently via the Sinkhorn algorithm (Cuturi, 2013), which alternates row and column normalizations in a matrix-scaling procedure. Despite its simplicity and scalability, it is a first-order method with sublinear convergence, meaning it often requires many iterations to reach high accuracy (Wang & Qiu, 2025). Recently, to speed up convergence, researchers have turned to second-order approaches like the Newton method (Tang & Qiu, 2024; Wang & Qiu, 2025; Tang et al., 2024). By combining Newton updates with sparse Hessian approximations and efficient linear solvers, these methods achieve fast local convergence and handle large datasets much better than standard Sinkhorn. However, the EOT solution remains only an approximation of the original OT problem. While reducing the regularization parameter improves approximation accuracy, excessively small regularization values cause the algorithm to slow down and lead to severe numerical instability, such as overflow and underflow.

Instead of settling for the approximate solution provided by EOT, recent research has shifted focus back to solving the original OT problem exactly. This is typically achieved by

viewing EOT (2) as a subproblem within a larger iterative framework, such as the Bregman proximal point algorithm. A natural approach is to solve these subproblems exactly until convergence. Wu et al. (2025) accelerated this process by applying Newton methods with sparsification techniques. However, requiring an exact solution at every step created a heavy computational burden. To reduce this cost, some inexact frameworks were introduced; these methods do not require solving the subproblem perfectly (Xie et al., 2020; Eckstein, 1998; Solodov & Svaiter, 2000). The limitation, however, is that verifying the stopping criterion for these methods is often theoretically difficult. Recently, (Yang & Toh, 2022) addressed this by proposing a new inexact framework with a stopping condition that is easy to verify. Motivated by this breakthrough, we utilize this inexact framework with efficient second-order Newton methods to achieve both high precision and computational efficiency.

In this paper, we propose an **Inexact Bregman Sparse Newton (IBSN)** framework for efficiently solving the original optimal transport problem (1). We construct subproblems based on Bregman divergence, while we further transform the subproblem into their semi-dual formulations. To improve overall efficiency, the subproblems are solved in exactly at each iteration. Moreover, to accelerate inner convergence, we employ a Newton-type refinement equipped with Hessian sparsification. By selectively retaining only the most significant entries of the Hessian, this technique drastically reduces computational overhead without sacrificing accuracy. By combining inexact Bregman updates with sparse Newton acceleration, IBSN achieves both high precision and scalability on large-scale datasets. Finally, we establish rigorous convergence guarantees for the algorithm and demonstrate its superior empirical performance compared to state-of-the-art methods.

Contribution The main contributions of this work are summarized as follows:

1. A Bregman Inexact Sparse Newton (IBSN) method is proposed for efficiently computing solutions with high accuracy to the original OT problem, where each subproblem is solved inexactly.
2. A Hessian sparsification scheme is introduced, which guarantees positive definiteness within a subspace and provides strict control over the induced approximation error.
3. Building on the sparsified Hessian, a Newton-type solver for the semi-dual subproblem is developed. This solver fully exploits the resulting sparse structure and achieves rapid convergence with substantially reduced computational cost.
4. We establish rigorous theoretical guarantees for the

proposed framework. Proofs of all theoretical results (Section 3- 4) are deferred to the Appendix B. We also conduct extensive numerical experiments demonstrating that IBSN consistently outperforms existing state-of-the-art methods in both accuracy and efficiency.

Notation For any $x \in \mathbb{R}^n$, we denote its i -th entry by x_i . For an index set $\mathcal{I} \subseteq [n] := \{1, 2, \dots, n\}$, $x_{\mathcal{I}} \in \mathbb{R}^{|\mathcal{I}|}$ represents the subvector of x corresponding to the indices in \mathcal{I} , where $|\mathcal{I}|$ denotes the cardinality of \mathcal{I} . The span of vector x is defined as $\text{span}\{x\} = \{cx : c \in \mathbb{R}\}$. We denote $\mathbf{1}_n$ and $\mathbf{0}_n$ as the n -dimensional vectors of all ones and all zeros, respectively. We use $\lambda_{\min}(\cdot)$ and $\lambda_{\max}(\cdot)$ to represent the smallest and largest eigenvalues of real symmetric matrices, respectively. For a matrix $A \in \mathbb{R}^{m \times n}$, let A_i be the vector of the i -th row of A . The kernel of matrix A is defined as $\ker(A) = \{x : Ax = \mathbf{0}_m\}$. We denote $\|\cdot\|_p$ as the ℓ_p norm of a vector or ℓ_p induced norm of a matrix. For simplicity, we use $\|\cdot\|$ to denote the Euclidean norm of a vector or the ℓ_2 induced norm of a matrix.

2. Related Work

Applications of OT The versatility of OT has led to its adoption in a broad range of scientific and engineering domains. In machine learning, OT distances underpin generative adversarial networks (Daniels et al., 2021; Arjovsky et al., 2017), domain adaptation (Courty et al., 2017b;a), and distributionally robust optimization (Onken et al., 2021) by offering geometry-aware measures of distributional discrepancy. In computer vision and graphics, OT provides a principled framework for color transfer (Rabin et al., 2014), texture mixing (Rabin et al., 2011), and point cloud registration (Shen et al., 2021; Puy et al., 2020). These diverse applications highlight the growing importance of efficient OT computation as a core building block for modern data science.

Computational OT Algorithmic advances in OT have followed two main directions. The first direction leverages entropy regularization for its computational benefits. Initial progress relied on first-order methods, most notably the Sinkhorn algorithm (Cuturi, 2013) and its variants (e.g., Greenhorn (Altschuler et al., 2017) and stabilized Sinkhorn (Schmitzer, 2019)). For further acceleration, Newton-based methods (as seen in (Tang & Qiu, 2024; Tang et al., 2024; Wang & Qiu, 2025; Brauer et al., 2017; Wu et al., 2025)) exploit second-order information and sparsity. The second direction tackles the original OT problem directly, often by embedding the EOT form into an iterative framework. The strategy of employing EOT as a subproblem within a Bregman framework is a natural and common approach. Other direct solvers include Halpern-accelerated approaches (HOT) (Zhang et al., 2025), primal-dual hybrid

gradient method (PDHG) (Applegate et al., 2021), Douglas-Rachford splitting algorithm (Mai et al., 2022), and extra-gradient method (Li et al., 2025).

Bregman proximal point Bregman divergence has been widely adopted as a proximal regularizer in large-scale optimization, particularly when the decision variables lie in the probability simplex (Bauschke et al., 2017; Beck & Teboulle, 2003; Bolte et al., 2018; Ben-Tal et al., 2001; Pan & Yan, 2025). Compared to Euclidean proximals, Bregman proximal mappings naturally encode the geometry of distributions and lead to algorithms with improved stability and interpretability.

Inexact optimization of inner subproblem A common strategy in large-scale optimization, including OT, is to solve inner subproblems only approximately rather than to full precision (Xie et al., 2020; Yang & Toh, 2022; Burachik et al., 1997; Eckstein, 1998). Such inexactness reduces per-iteration cost while still guaranteeing global convergence, provided that the approximation error is controlled relative to the outer iteration.

3. Methodology

This section details the Inexact Bregman Sparse Newton (IBSN) framework, a Newton-type scheme for solving the original OT problem (1). We begin by introducing the subproblem formulation and its corresponding semi-dual problem based on Bregman divergence in Section 3.1. Next, in Section 3.2, we describe the Hessian sparsification strategy designed to enhance computational efficiency. Finally, Section 3.3 outlines the complete algorithmic framework, detailing the inexact Newton update mechanism and overall procedure.

3.1. Subproblem formulation

To compute the optimal transport plan, we employ a Bregman proximal point framework. In this iterative scheme, each iteration solves a regularized subproblem of the form:

$$X^{k+1} \in \arg \min_{X \in \Omega} \{ \langle C, X \rangle + \eta D_\phi(X, X^k) \}, \quad (3)$$

where $D_\phi(X, Y) = \sum_{i,j} X_{ij} \log \frac{X_{ij}}{Y_{ij}} - \sum_{i,j} X_{ij} + \sum_{i,j} Y_{ij}$ is the Bregman divergence based on the negative entropy function ϕ . It has been shown that the subproblem (3) can be equivalently stated via its two-dual formulation (Tang & Qiu, 2024):

$$\begin{aligned} \min_{\gamma \in \mathbb{R}^n, \zeta \in \mathbb{R}^m} Z^k(\gamma, \zeta) &:= -\mathbf{a}^\top \zeta - \mathbf{b}^\top \gamma \\ &+ \eta \sum_{i=1}^m \sum_{j=1}^n X_{ij}^k \exp\{(\zeta_i + \gamma_j - C_{ij})/\eta\}. \end{aligned} \quad (4)$$

Under this framework, the Sinkhorn algorithm can be interpreted as a simple alternating minimization algorithm that iteratively minimizes $Z^k(\gamma, \zeta)$ with respect to γ and ζ .

To simplify the optimization landscape, especially for our Newton-type method, we work with the semi-dual formulation. This form is derived by eliminating one set of dual variables. Without loss of generality, we proceed to eliminate the dual variable ζ by letting $\frac{\partial Z^k(\gamma, \zeta)}{\partial \zeta} = \mathbf{0}_m$, i.e.,

$$\zeta(\gamma)_i = \eta \log a_i - \eta \log \left(\sum_{j=1}^n X_{ij}^k \exp\{(\gamma_j - C_{ij})/\eta\} \right). \quad (5)$$

Substituting this back into the two-dual problem (4), we obtain the semi-dual formulation which minimizes over only γ :

$$\begin{aligned} \min_{\gamma \in \mathbb{R}^n} \mathcal{L}^k(\gamma) &:= - \sum_{j=1}^n \gamma_j b_j \\ &+ \eta \sum_{i=1}^m a_i \log \left(\sum_{j=1}^n X_{ij}^k \exp((\gamma_j - C_{ij})/\eta) \right). \end{aligned} \quad (6)$$

The following lemma guarantees the existence of an optimal solution for this formulation (6).

Lemma 3.1. *The semi-dual problem (6) has a solution.*

Let $\gamma^{k,*}$ denote an optimal solution to (6), then the corresponding primal update X^{k+1} can be recovered via $X^{k+1} = \text{diag}(\mathbf{a}) P^k(\gamma^{k,*})$, where $P^k(\gamma)$ is a matrix with entries:

$$[P^k(\gamma)]_{ij} = \frac{X_{ij}^k \exp((\gamma_j - C_{ij})/\eta)}{\sum_{l=1}^n X_{il}^k \exp((\gamma_l - C_{il})/\eta)}. \quad (7)$$

The partial gradient g^k of $\mathcal{L}^k(\gamma)$ with respect to γ and its corresponding Hessian matrix H^k are given by

$$\begin{aligned} g^k(\gamma) &= (P^k(\gamma))^\top \mathbf{a} - \mathbf{b}, \\ H^k(\gamma) &= \frac{1}{\eta} (\text{diag}(P^k(\gamma)^\top \mathbf{a}) - P^k(\gamma)^\top \text{diag}(\mathbf{a}) P^k(\gamma)). \end{aligned} \quad (8)$$

This highly smooth and structured formulation provides major advantages for using Newton methods to solve (6). First, the existence and easy computation of the Hessian enables the use of Newton method. This guarantees a much faster rate of convergence compared to the sublinear convergence typical of first-order algorithms like Sinkhorn. Second, compared to the classical two-dual formulation, this approach reduces the number of dual variables from $(m+n)$ to n . This significantly lowers the memory requirement for the Hessian matrix (from $(m+n) \times (m+n)$ to $n \times n$) and reduces the computational effort for computing the Newton direction. Third, the inherent structure of the Hessian is

ideally suited for the sparsification technique we detail in the next subsection. This mathematical property is key to reducing the computational cost without sacrificing accuracy.

3.2. Sparsifying the Hessian matrix

In this subsection, we detail our strategy for accelerating the process that uses to compute the Newton directions. For brevity, in the current subproblem iteration k , we denote the matrix, gradient and Hessian by $P = P^k(\gamma)$, $\mathbf{g} = g^k(\gamma)$ and $H = H^k(\gamma)$, respectively in this subsection.

The classical Newton method requires solving the linear system $H(\Delta\gamma) = -\mathbf{g}$. However, computing this solution directly is prohibitively expensive for large-scale OT problems, especially for the dense matrix. The key insight that allows us to bypass this cost is the structure of the solution: the optimal transport plan is often inherently sparse. While the exact Hessian H is formally dense in the iteration, its structure is closely related to the transport plan, suggesting that a sparse approximation is both reasonable and highly beneficial. Therefore, we introduce a Hessian sparsification technique to approximate H and significantly reduce the required computation.

Our strategy constructs a ‘sparse’ approximation H_ρ of the exact Hessian H . This approach is simple and leverages the structure inherent in the definition of H and the intermediate matrix P . We achieve sparsification by retaining only the dominant elements of P . A subsequent normalization step is then applied to ensure the row sums are preserved (i.e., sum of each row remains 1). This approach produces a sparse approximation that preserves accuracy while significantly lowering the cost of the Newton updates. We detail the specific thresholding and normalization steps for constructing H_ρ in Algorithm 1.

Algorithm 1 Sparsifying the Hessian matrix

- 1: **Input:** Outer iteration k , dual variable γ , threshold parameter $\rho \geq 0$, $i^* = \arg \max_{i \in [m]} a_i$.
- 2: Compute $P \leftarrow P^k(\gamma)$ using (7).
- 3: Construct the sparsified matrix P_ρ by setting

$$[P_\rho]_{ij} \leftarrow \frac{P_{ij} \mathbf{1}_{\{P_{ij} \geq \rho\}}}{\sum_{k=1}^n P_{ik} \mathbf{1}_{\{P_{ik} \geq \rho\}}} \quad \forall i \neq i^*, [P_\rho]_{i^*} \leftarrow P_{i^*}.$$

- 4: Compute $H_\rho \leftarrow (\text{diag}(P_\rho^\top \mathbf{a}) - P_\rho^\top \text{diag}(\mathbf{a}) P_\rho) / \eta$.
 - 5: **Output:** H_ρ .
-

This construction naturally raises two important questions. First, **is H_ρ invertible?** This property is crucial for implementing the Newton step, as computing the direction $\Delta\gamma$ requires solving the linear system $H_\rho(\Delta\gamma) = -\mathbf{g}$. Ensuring invertibility guarantees that the system admits a unique solution and that the Newton direction is well defined. Second,

how accurate is H_ρ as an approximation of the true Hessian H ? A quantitative understanding of this discrepancy guides the choice of the sparsification threshold ρ , balancing computational efficiency with approximation accuracy.

To address these questions, we first establish the structural properties of H_ρ . The following result shows that the sparsified Hessian constructed by Algorithm 1 remains positive definite on the feasible subspace, ensuring that the Newton step is always well defined.

Theorem 3.2. *The matrix H_ρ output by Algorithm 1 is symmetric and positive semidefinite, and its kernel satisfies $\ker(H_\rho) = \text{span}\{\mathbf{1}_n\} \forall \rho \geq 0$.*

Theorem 3.2 implies that, for any $\rho \geq 0$, H_ρ is positive definite on the orthogonal complement $\mathbf{1}_n^\perp$ of the kernel. Note that the gradient \mathbf{g} satisfies $\mathbf{1}_n^\top \mathbf{g} = 0$, so the Newton system can be efficiently solved using the conjugate gradient (CG) method. In particular, the CG iterates are guaranteed to remain within $\mathbf{1}_n^\perp$ as long as the initial iterate is chosen from $\mathbf{1}_n^\perp$, a fact that will be established in the next section.

We next characterize the spectral properties of the sparsified Hessian H_ρ , which are vital for establishing the convergence rate of the overall algorithm.

Theorem 3.3. *Let H_ρ be the matrix output by Algorithm 1 and let $(H_\rho)|_{\mathbf{1}_n^\perp}$ denote its restriction to the subspace $\mathbf{1}_n^\perp$, then $\forall \rho \geq 0$,*

$$\lambda_{\min}((H_\rho)|_{\mathbf{1}_n^\perp}) \geq n a_{i^*} p^2 / \eta, \quad \lambda_{\max}(H_\rho) \leq 1 / (2\eta),$$

where $p := \min_j [P]_{i^*j}$.

These bounds ensure that H_ρ is well-conditioned on the feasible subspace, providing stability for the Newton update and reliable convergence behavior across different sparsification levels.

To address the second question regarding accuracy, we establish a quantitative bound on the approximation error between the exact and sparsified Hessians.

Theorem 3.4. *Let H_ρ be the matrix output by Algorithm 1, then*

$$\|H - H_\rho\| \leq \frac{6mn \|\mathbf{a}\|_\infty}{\eta} \rho.$$

Theorem 3.4 shows that the approximation error increases with the problem size m, n and decreases with the regularization parameter η . To maintain a small and stable error across different scales, the threshold ρ can be chosen proportional to $\eta / (mn)$. This choice balances sparsity and accuracy while ensuring consistent performance as m, n , or η vary.

The preceding analysis confirms that the Hessian sparsification technique constructed via Algorithm 1 yields an

Algorithm 2 Inexact Bregman Sparse Newton (IBSN)

```

1: Input: Initial  $X^0 = \mathbf{a}\mathbf{b}^\top$ ,  $\gamma^{0,0} = \mathbf{0}_n$ ,  $\zeta^{0,0} = \mathbf{0}_m$ ,
    $\{\mu_k\}_k$ ,  $\eta$ , Armijo parameter  $\sigma = 10^{-4}$ ,  $\beta = 0.8$ .
2: for  $k = 0, \dots, K - 1$  do
3:   Solve the dual subproblem (4) starting from
    $\gamma^{k,0}, \zeta^{k,0}$  using Sinkhorn algorithm to obtain a
   coarse solution  $\gamma^{k,1}, \zeta^{k,1}$ .
4:   Update  $\gamma^{k,1} \leftarrow \gamma^{k,1} - \frac{1}{n} \mathbf{1}_n^\top \gamma^{k,1} \mathbf{1}_n$ .
5:   for  $v = 1, 2, \dots$  do
6:     Compute the gradient  $\mathbf{g}^{k,v} = \mathbf{g}^k(\gamma^{k,v})$  and update
     the sparsification threshold  $\rho \leftarrow \frac{\eta}{mn} \|\mathbf{g}^{k,v}\|$ .
7:     Construct  $H_\rho^{k,v}$  by Algorithm 1.
8:     Compute  $\Delta\gamma^{k,v} \leftarrow - (H_\rho^{k,v} + \|\mathbf{g}^{k,v}\|I)^{-1} \mathbf{g}^{k,v}$ .
9:     Select the stepsize  $t^{k,v}$  by Armijo backtracking.
10:    Compute  $\gamma^{k,v+1} \leftarrow \gamma^{k,v} + t^{k,v} \Delta\gamma^{k,v}$ .
11:    Compute  $X^{k,v+1} \leftarrow \text{diag}(\mathbf{a}) P^k(\gamma^{k,v+1})$ .
12:    if  $D_\phi(\mathcal{P}_\Omega(X^{k,v+1}), X^{k,v+1}) \leq \mu_k$  then
13:      Obtain  $X^{k+1} \leftarrow X^{k,v+1}$ ,  $\gamma^{k+1,0} \leftarrow \gamma^{k,v+1}$ .
14:      Calculate  $\zeta^{k+1,0}$  by (5) and break.
15:    end if
16:  end for
17: end for
18: Output:  $X^K$ .

```

approximation H_ρ that is both structurally robust and quantitatively accurate. However, even with these sparsification and second-order acceleration techniques, solving the problem (6) to high precision in every iteration remains computationally prohibitive. To fully address this efficiency bottleneck, we adopt the inexact Bregman framework proposed by (Yang & Toh, 2022). This framework allows the subproblems (3) to be solved approximately while still ensuring global convergence to the optimal OT solution. The details of this inexact criterion and its integration into our method are shown in the next subsection.

3.3. The proposed algorithm

We propose Algorithm 2, the Inexact Bregman Sparse Newton, an inexact framework that efficiently solves the OT problem (1) using a Newton-type approach with Hessian sparsification.

At each outer iteration k , the algorithm starts with Sinkhorn algorithm to approximately solve the subproblem (4). This generates a coarse estimate $\gamma^{k,1}$ that serves as a high-quality warm start for the subsequent Newton steps.

Within each inner iteration v , the algorithm computes the gradient $\mathbf{g}^{k,v}$ of \mathcal{L}^k and adaptively updates the sparsification threshold parameter ρ . Specifically, when the current iterate $\gamma^{k,v}$ is far away from the optimum with large $\|\mathbf{g}^{k,v}\|$, a larger ρ is chosen. This yields a sparser Hessian

$H_\rho^{k,v}$, which significantly reduces the computational burden of solving for the Newton direction $\Delta\gamma^{k,v}$. As $\gamma^{k,v}$ approaches the optimum with smaller $\|\mathbf{g}^{k,v}\|$, the threshold ρ progressively decreases. Therefore, $H_\rho^{k,v}$ becomes a more accurate approximation of the true Hessian $H^{k,v}$, achieving a faster local convergence rate.

To stabilize the Newton update and maintain a descent direction, a shift parameter proportional to the gradient norm, $\|\mathbf{g}^{k,v}\|$, is introduced into the linear system. This modification ensures numerical stability and guarantees that $\Delta\gamma^{k,v}$ is a descent direction for \mathcal{L}^k , as rigorously shown in Section 4. This shift naturally diminishes as $\gamma^{k,v}$ approaches the optimum. Such similar modifications have been adopted in recent Newton-type OT solvers (Tang & Qiu, 2024; Wang & Qiu, 2025).

After determining the step size $t^{k,v}$ through Armijo backtracking, the dual variable is updated, and the corresponding primal transport plan is updated as $X^{k,v+1} = \text{diag}(\mathbf{a}) P^k(\gamma^{k,v+1})$. To improve efficiency, the algorithm employs an inexact inner stopping criterion based on the Bregman divergence D_ϕ and the projection operator \mathcal{P}_Ω , which is the key component of the inexact framework in (Yang & Toh, 2022). Specifically, the inner loop terminates early once the condition

$$D_\phi(\mathcal{P}_\Omega(X^{k,v+1}), X^{k,v+1}) \leq \mu_k$$

is satisfied, where μ_k represents the inexactness tolerance. After this, $X^{k,v+1}$ and $\gamma^{k,v+1}$ are propagated as the initialization for the next outer iteration. This adaptive inexactness substantially reduces computational cost while preserving theoretical convergence guarantees. In practice, the rounding procedure proposed in (Altschuler et al., 2017) can also be used as an efficient approximation of \mathcal{P}_Ω , further improving scalability in large-scale settings (see Appendix A).

In summary, the IBSN algorithm unifies the efficiency of inexact Bregman updates with the acceleration of sparse Newton refinements to achieve high accuracy and scalability when solving large-scale OT problems.

4. Theoretical Analysis

This section presents the convergence analysis of the proposed IBSN framework. We first establish the inner convergence of the Newton iterations with sparsified Hessians, followed by proving the global convergence of the outer iterations to the exact optimal transport solution.

4.1. Inner convergence analysis

This subsection establishes the crucial convergence properties of the inner iterations within the IBSN framework, demonstrating that our sparse Newton steps successfully find the unique solution to each subproblem. We start with

the following lemma, which validates our approach by confirming that the entire optimization sequence remains confined to this desirable subspace.

Lemma 4.1. *Let $\{\gamma^{k,v}\}$ be the sequence generated by Algorithm 2 with $\mathbf{1}_n^\top \gamma^{0,0} = 0$, then $\mathbf{1}_n^\top \gamma^{k,v} = 0$ for $\forall k, v$.*

Lemma 4.1 ensures that the convergence analysis can be safely restricted to the subspace $\mathbf{1}_n^\perp$, effectively eliminating the redundant degree of freedom and restoring the strong convexity of \mathcal{L}^k .

We then establish that the inner iterates $\gamma^{k,v}$ generated by Algorithm 2 converge to the unique global minimizer of \mathcal{L}^k within the subspace $\mathbf{1}_n^\perp$.

Theorem 4.2. *For a fixed outer k -th iteration, let $\{\gamma^{k,v}\}_v$ be the sequence generated by Algorithm 2 with $\mathbf{1}_n^\top \gamma^{k,0} = 0$, then the following holds:*

- (i) $\|\mathbf{g}^{k,v}\| \rightarrow 0$ as $v \rightarrow \infty$.
- (ii) $\gamma^{k,v} \rightarrow \gamma^{k,*}$, where $\gamma^{k,*}$ is the unique minimizer of \mathcal{L}^k in the slice $\{\gamma : \mathbf{1}_n^\top \gamma = 0\}$.

Next, we examine the highly favorable local convergence rate achieved by the sparse Newton iterations.

Theorem 4.3. *For a fixed outer k -th iteration, let $\gamma^{k,*}$ denote the unique solution in the slice $\{\gamma : \mathbf{1}_n^\top \gamma = 0\}$ of \mathcal{L}^k . Assume that $H^{k,v}$ is Lipschitz continuous with constant L_H in a neighborhood of $\gamma^{k,*}$, and that $t^{k,v} = 1$ is accepted, then there exists a constant $L > 0$ such that*

$$\|\gamma^{k,v+1} - \gamma^{k,*}\| \leq L \|\gamma^{k,v} - \gamma^{k,*}\|^2. \quad (9)$$

Together, Theorems 4.2 and 4.3 establish that the proposed sparse Newton updates converge globally to the unique solution of each subproblem and exhibit quadratic local convergence once sufficiently close to the optimum. This demonstrates that the sparsified Newton steps preserve the accuracy and convergence speed of the classical method, making this approach feasible for large-scale optimal transport problem.

4.2. Global convergence

We now establish the global convergence of the proposed IBSN algorithm. Let $f(X) = \langle C, X \rangle$ and $f^* = \min\{f(X) : X \in \Omega\}$. Our convergence proof relies on the principles of the inexact Bregman proximal point algorithm, adapted from the results established in (Yang & Toh, 2022).

Proposition 4.4. *((Yang & Toh, 2022)) Let $\{X^k\}$ be the sequence generated by the Algorithm 2. If $\sum_k \mu_k < \infty$, then $f(\mathcal{P}_\Omega(X^k)) \rightarrow f^*$ as $k \rightarrow \infty$ and both sequence $\{X^k\}$ and $\{\mathcal{P}_\Omega(X^k)\}$ converge to the same limit, which is an optimal solution of problem (1).*

This result establishes the global convergence of IBSN under mild conditions on the inexactness tolerance μ_k . It confirms that the combination of inexact subproblem solving and sparse Newton acceleration does not compromise the overall theoretical accuracy, ensuring that the proposed algorithm converges to the exact optimal transport plan.

5. Numerical Experiments

In this section, we evaluate the performance of the proposed IBSN algorithm through a series of numerical experiments on both synthetic and real datasets and compare its empirical performance with existing state-of-the-art optimal transport solvers: 1. PINS algorithm (Wu et al., 2025); 2. HOT algorithm (Zhang et al., 2025); 3. Inexact Bregman framework with Sinkhorn (IBSink) (Yang & Toh, 2022); 4. IPOT algorithm (Xie et al., 2020); 5. Extragradients (ExtraGrad) method (Li et al., 2025). All numerical experiments are implemented in Python 3.9.18 on a MacBook Pro running macOS 13.0 with an Apple M2 Pro processor and 16 GB RAM.

Setup To ensure consistency, we normalize all cost matrices to have a unit infinity norm, i.e., $C \leftarrow C / \max_{i,j} |C_{ij}|$. We initialize the transport plan as $X^0 = \mathbf{a}\mathbf{b}^\top$.

We use the relative KKT residual (Yang & Toh, 2022) (Δ_{kkt}) as the unified stopping criterion for all methods (see Appendix C.1). An algorithm is terminated once $\Delta_{\text{kkt}} < 10^{-11}$ or the maximum number of iterations is attained.

Within the inner iteration of IBSN, the Sinkhorn warm-up phase stops once the gradient norm is less than 10^{-3} . In addition, we terminate the Newton phase when

$$D_\phi(\mathcal{P}_\Omega(X^{k+1}), X^{k+1}) \leq \min\{m, n\} \cdot \mu_k, \quad (10)$$

where $\mu_k = \max\{10^{-4}/(k+1)^2, 10^{-11}\}$,

where \mathcal{P}_Ω is computed using the rounding procedure in (Altschuler et al., 2017). To save computational time, we only evaluate the condition (10) after a simpler gradient norm check ($\|\nabla \mathcal{L}^k(\gamma^{k,v+1})\| < \mu_k$) passes (as suggested in (Yang & Toh, 2022)).

To compare the solution quality, we utilize the objective gap relative to a high-precision ground truth X^* (obtained via Gurobi with tolerance 10^{-8}):

$$\text{Gap} = |\langle C, \mathcal{P}_\Omega(X) \rangle - \langle C, X^* \rangle|.$$

5.1. Synthetic data

We generate synthetic datasets using the following procedure. The marginal distributions \mathbf{a} and \mathbf{b} are sampled independently from a uniform distribution on $(0, 1)$ and subsequently normalized to satisfy $\mathbf{1}_m^\top \mathbf{a} = \mathbf{1}_n^\top \mathbf{b} = 1$. We

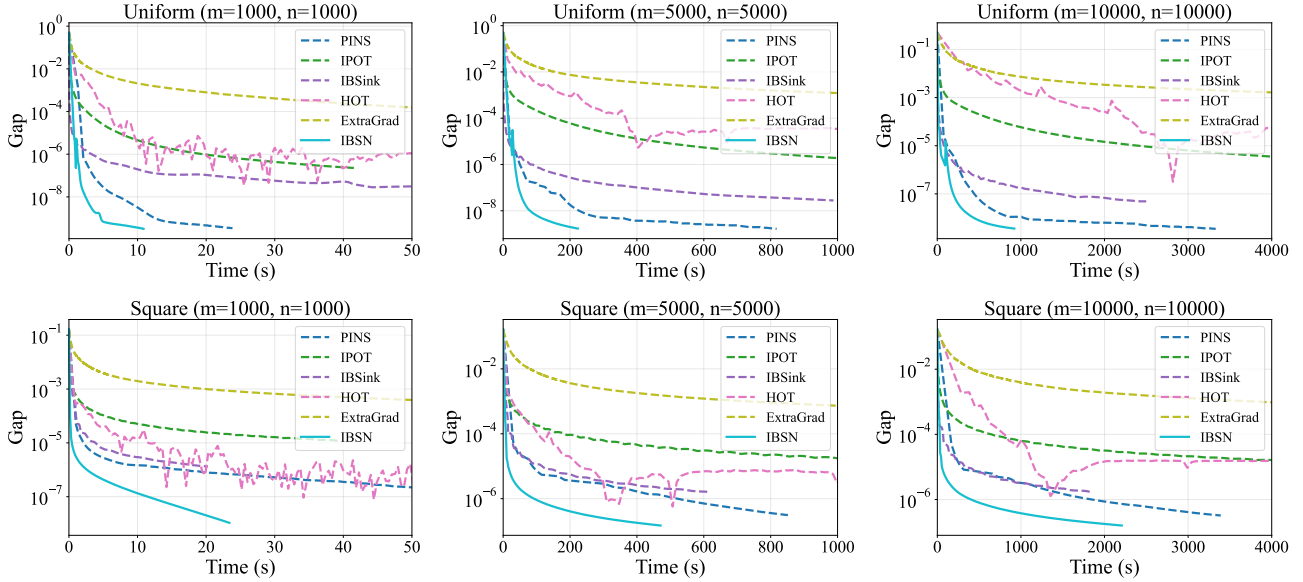


Figure 1. Performance of different algorithms on synthetic data. Top: Uniform setting. Bottom: Square setting.

evaluate performance across problem dimensions $m = n \in \{1000, 5000, 10000\}$ using two types of cost matrices:

- **Uniform:** Each entry of C is drawn independently from the uniform distribution on $(0, 1)$.
- **Square:** The cost matrix $C \in \mathbb{R}^{m \times n}$ is defined by the squared ℓ_2 -distance between pixel indices, i.e., $C_{ij} = (i - j)^2$.

We set $\eta = 10^{-4}$ for both IBSN and PINS, $\eta = 10^{-3}$ for IBSink, $\eta = 10^{-1}$ for IPOT. These values are selected based on empirical tuning and correspond to the best observed trade-off between convergence speed and solution accuracy for each method. A more detailed analysis of the impact of the regularization parameter η is provided in Appendix C.2.

The experimental results are presented in Figure 1. The second-order methods (IBSN and PINS) have faster convergence speed compared with the first-order methods in most cases. This takes advantage of using sparse matrix operations to reduce its per-iteration cost and fast convergence speed of second-order methods. In addition, IBSN surpasses PINS in overall efficiency. This advantage stems from our semi-dual formulation, which further reduces the cost of the second-order updates.

5.2. Real data

We further evaluate the proposed IBSN algorithm on real-image OT tasks to examine its effectiveness in practical scenarios. Two benchmark datasets are considered:

- **(Fashion-)MNIST:** We compute the OT map between

pairs of images from the MNIST (LeCun et al., 2002) and the Fashion-MNIST (Xiao et al., 2017) datasets. The vectors \mathbf{a} and \mathbf{b} are obtained by flattening and normalizing the pixel intensity values, while the cost matrix C is generated via the squared ℓ_2 -distance between pixel indices. The problem size is set to $m = n = 784$.

- **DOTmark:** The DOTmark dataset (Schrieber et al., 2016) provides a comprehensive benchmark suite for evaluating OT algorithms. In our experiments, we select two images each from three categories (Shapes, ClassicImages, WhiteNoise) in the dataset, with image size 32×32 ($m = n = 1024$) and 64×64 ($m = n = 4096$). The cost matrix C and marginal vectors \mathbf{a}, \mathbf{b} are constructed in the same manner as in the (Fashion-)MNIST experiments.

We set $\eta = 10^{-3}$ for IBSN, PINS and IBSink, $\eta = 10^{-1}$ for IPOT. These choices of η are determined in the same way as in Section 5.1.

Figure 2 shows the results on the (Fashion-)MNIST dataset. As observed, first-order methods (HOT and ExtraGrad) remain comparatively slow. Notably, the convergence trajectory of IBSink exhibits three distinct stages, a behavior attributable to the inexact framework. Initially, the algorithm converges rapidly due to the loose inexactness tolerance μ_k . As the tolerance tightens, IBSink enters a second stage where it requires significantly more iterations to satisfy the inner stopping criterion, causing a slowdown. Finally, as the transport plan X approaches the optimal X^* , convergence accelerates again. In contrast, our proposed IBSN algorithm overcomes this mid-stage bottleneck by leveraging

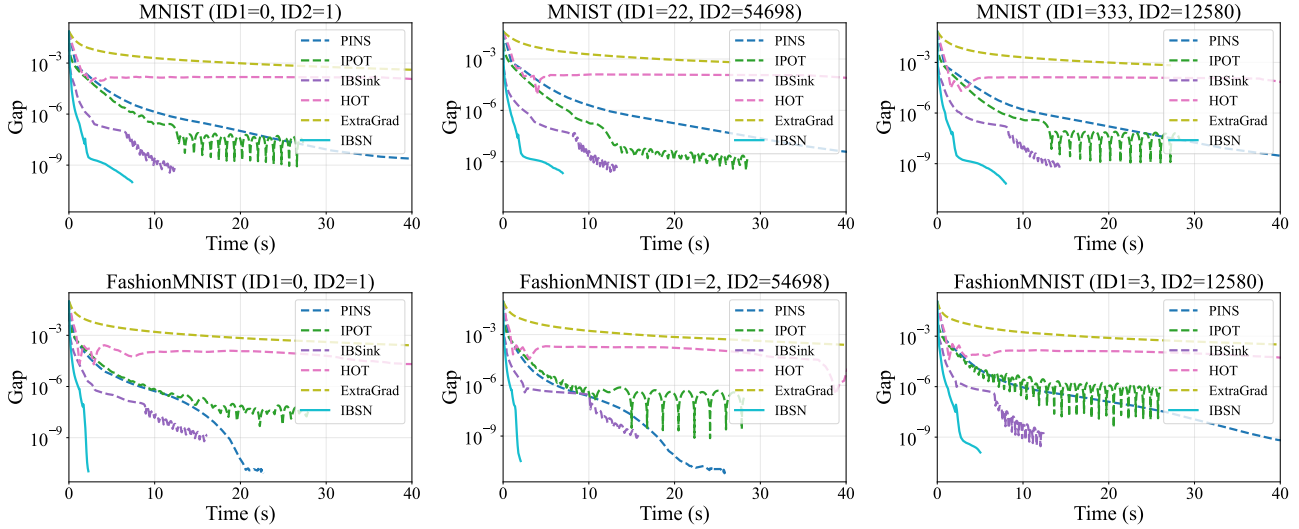


Figure 2. Performance of different algorithms on MNIST dataset (Top) and Fashion-MNIST dataset (Bottom).

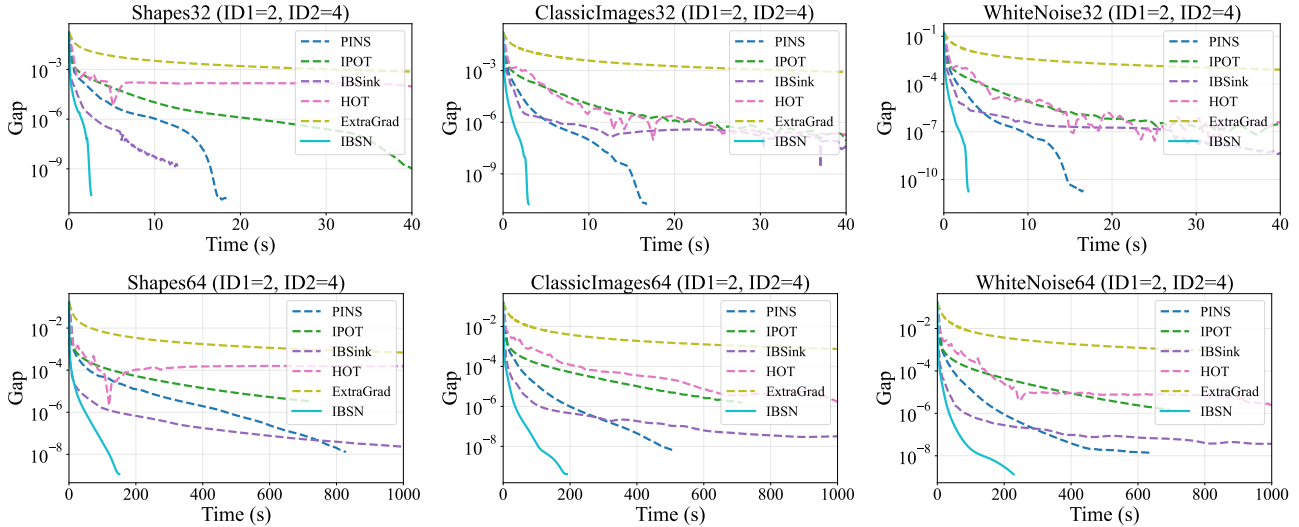


Figure 3. Performance of different algorithms on DOTmark dataset. Top: Image size 32×32 . Bottom: Image size 64×64 .

second-order information. This allows it to maintain rapid convergence even when the tolerance μ_k becomes strict. Similar patterns are observed in the DOTmark dataset results (Figure 3), where the performance gap between IBSN and competing algorithms is even more pronounced. More experiment results are given in Appendix C.

6. Conclusion

In this paper, we presented the Inexact Bregman Sparse Newton (IBSN) method, a novel framework for efficiently solving the exact optimal transport problem. By converting the subproblem into a semi-dual formulation and applying a Hessian sparsification strategy, our approach significantly reduces the computational cost associated with second-order

updates. Furthermore, we employ a verifiable inexact stopping criterion, which allows the algorithm to proceed without solving every subproblem to high precision while still ensuring global convergence to the optimal plan. Our theoretical analysis confirms the convergence of the method, and extensive experiments on both synthetic and real-world datasets demonstrate that IBSN outperforms existing state-of-the-art solvers in terms of both speed and accuracy.

Impact Statement

This paper presents work whose goal is to advance the field of Machine Learning. There are many potential societal consequences of our work, none of which we feel must be specifically highlighted here.

References

- Altschuler, J. M., Weed, J., and Rigollet, P. Near-linear time approximation algorithms for optimal transport via Sinkhorn iteration. In *Advances in Neural Information Processing Systems*, volume 30, pp. 1964–1974, 2017.
- Amos, B., Luise, G., Cohen, S., and Redko, I. Meta Optimal Transport. In *Proceedings of the 40th International Conference on Machine Learning*, volume 202, pp. 791–813. PMLR, 2023.
- Applegate, D., Díaz, M., Hinder, O., Lu, H., Lubin, M., O’Donoghue, B., and Schudy, W. Practical large-scale linear programming using primal-dual hybrid gradient. In *Advances in Neural Information Processing Systems*, volume 34, pp. 20243–20257, 2021.
- Arjovsky, M., Chintala, S., and Bottou, L. Wasserstein generative adversarial networks. In *Proceedings of the 34th International Conference on Machine Learning*, volume 70, pp. 214–223. PMLR, 2017.
- Bauschke, H. H., Bolte, J., and Teboulle, M. A descent lemma beyond Lipschitz gradient continuity: First-order methods revisited and applications. *Mathematics of Operations Research*, 42(2):330–348, 2017.
- Beck, A. and Teboulle, M. Mirror descent and nonlinear projected subgradient methods for convex optimization. *Operations Research Letters*, 31(3):167–175, 2003.
- Ben-Tal, A., Margalit, T., and Nemirovski, A. The ordered subsets mirror descent optimization method with applications to tomography. *SIAM Journal on Optimization*, 12(1):79–108, 2001.
- Blondel, M., Seguy, V., and Rolet, A. Smooth and sparse optimal transport. In *Proceedings of the 21st International Conference on Artificial Intelligence and Statistics*, volume 84, pp. 880–889. PMLR, 2018.
- Bolte, J., Sabach, S., Teboulle, M., and Vaisbourd, Y. First order methods beyond convexity and Lipschitz gradient continuity with applications to quadratic inverse problems. *SIAM Journal on Optimization*, 28(3):2131–2151, 2018.
- Bonneel, N. and Digne, J. A survey of optimal transport for computer graphics and computer vision. In *Computer Graphics Forum*, volume 42, pp. 439–460. Wiley Online Library, 2023.
- Brauer, C., Clason, C., Lorenz, D., and Wirth, B. A Sinkhorn-Newton method for entropic optimal transport. *arXiv preprint arXiv:1710.06635*, 2017.
- Burachik, R. S., Iusem, A. N., and Svaiter, B. F. Enlargement of monotone operators with applications to variational inequalities. *Set-Valued Analysis*, 5(2):159–180, 1997.
- Burkard, R., Dell’Amico, M., and Martello, S. *Assignment problems: revised reprint*. SIAM, 2012.
- Courty, N., Flamary, R., Habrard, A., and Rakotomamonjy, A. Joint distribution optimal transportation for domain adaptation. In *Advances in Neural Information Processing Systems*, volume 30, pp. 3730–3739, 2017a.
- Courty, N., Flamary, R., Tuia, D., and Rakotomamonjy, A. Optimal transport for domain adaptation. *IEEE Transactions on Pattern Analysis and Machine Intelligence*, 39(9):1853–1865, 2017b.
- Cuturi, M. Sinkhorn distances: Lightspeed computation of optimal transport. In *Advances in Neural Information Processing Systems*, volume 26, pp. 2292–2300, 2013.
- Daniels, G., Maunu, T., and Hand, P. Score-based generative neural networks for large-scale optimal transport. In *Advances in Neural Information Processing Systems*, volume 34, pp. 12955–12965, 2021.
- Doxsey-Whitfield, E., MacManus, K., Adamo, S. B., Pistolesi, L., Squires, J., Borkovska, O., and Baptista, S. R. Taking advantage of the improved availability of census data: a first look at the gridded population of the world, version 4. *Papers in Applied Geography*, 1(3):226–234, 2015.
- Dvurechensky, P. E., Gasnikov, A. V., and Kroshnin, A. Computational optimal transport: Complexity by accelerated gradient descent is better than by Sinkhorn’s algorithm. In *Proceedings of the 35th International Conference on Machine Learning*, volume 80, pp. 1366–1375. PMLR, 2018.
- Eckstein, J. Approximate iterations in Bregman-function-based proximal algorithms. *Mathematical Programming*, 83(1):113–123, 1998.
- Flamary, R., Courty, N., Gramfort, A., Alaya, M. Z., Boissunon, A., Chambon, S., Chapel, L., Corenflos, A., Fatras, K., Fournier, N., Gautheron, L., Gayraud, N. T., Janati, H., Rakotomamonjy, A., Redko, I., Rolet, A., Schutz, A., Seguy, V., Sutherland, D. J., Tavenard, R., Tong, A., and Vayer, T. Pot: Python optimal transport. *Journal of Machine Learning Research*, 22(78):1–8, 2021.
- Flamary, R., Vincent-Cuaz, C., Courty, N., Gramfort, A., Kachaiev, O., Quang Tran, H., David, L., Bonet, C., Cassereau, N., Gnassounou, T., Tanguy, E., Delon, J., Collas, A., Mazelet, S., Chapel, L., Kerdoncuff, T., Yu, X.,

- Feickert, M., Krzakala, P., Liu, T., and Fernandes Montesuma, E. Pot python optimal transport (version 0.9.5), 2024.
- Goldfeld, Z., Kato, K., Rioux, G., and Sadhu, R. Statistical inference with regularized optimal transport. *Information and Inference: A Journal of the IMA*, 13(1):iaad056, 2024.
- Gordaliza, P., Del Barrio, E., Fabrice, G., and Loubes, J.-M. Obtaining fairness using optimal transport theory. In *International conference on machine learning*, pp. 2357–2365. PMLR, 2019.
- Klatt, M., Tameling, C., and Munk, A. Empirical regularized optimal transport: Statistical theory and applications. *SIAM Journal on Mathematics of Data Science*, 2(2): 419–443, 2020.
- LeCun, Y., Bottou, L., Bengio, Y., and Haffner, P. Gradient-based learning applied to document recognition. *Proceedings of the IEEE*, 86(11):2278–2324, 2002.
- Li, G., Chen, Y., Huang, Y., Chi, Y., Poor, H. V., and Chen, Y. Fast computation of optimal transport via entropy-regularized extragradient methods. *SIAM Journal on Optimization*, 35(2):1330–1363, 2025.
- Liu, T., Puigcerver, J., and Blondel, M. Sparsity-constrained optimal transport. In *The Eleventh International Conference on Learning Representations*, 2023.
- Mai, V. V., Lindbäck, J., and Johansson, M. A fast and accurate splitting method for optimal transport: analysis and implementation. In *The International Conference on Learning Representations*, 2022.
- Montesuma, E. F., Mboula, F. M. N., and Souloumiac, A. Recent advances in optimal transport for machine learning. *IEEE Transactions on Pattern Analysis and Machine Intelligence*, 47(2):1161–1180, 2024.
- Nesterov, Y. and Nemirovskii, A. *Interior-point polynomial algorithms in convex programming*. SIAM, 1994.
- Nesterov, Y. et al. *Lectures on convex optimization*, volume 137. Springer, 2018.
- Oneto, L., Donini, M., Luise, G., Ciliberto, C., Maurer, A., and Pontil, M. Exploiting MMD and Sinkhorn divergences for fair and transferable representation learning. *Advances in Neural Information Processing Systems*, 33: 15360–15370, 2020.
- Onken, D., Fung, S. W., Li, X., and Ruthotto, L. OT-Flow: Fast and accurate continuous normalizing flows via optimal transport. In *Proceedings of the AAAI Conference on Artificial Intelligence*, volume 35, pp. 9223–9232, 2021.
- Pan, J. and Yan, M. Efficient sparse probability measures recovery via bregman gradient. *Journal of Scientific Computing*, 102(3):66, 2025.
- Puy, G., Boulch, A., and Marlet, R. Flot: Scene flow on point clouds guided by optimal transport. In *European conference on computer vision*, pp. 527–544. Springer, 2020.
- Rabin, J., Peyré, G., Delon, J., and Bernot, M. Wasserstein barycenter and its application to texture mixing. In *International conference on scale space and variational methods in computer vision*, pp. 435–446. Springer, 2011.
- Rabin, J., Ferradans, S., and Papadakis, N. Adaptive color transfer with relaxed optimal transport. In *2014 IEEE International Conference on Image Processing (ICIP)*, pp. 4852–4856. IEEE, 2014.
- Rakotomamonjy, A., Flamary, R., and Courty, N. Generalized conditional gradient: analysis of convergence and applications. *arXiv preprint arXiv:1510.06567*, 2015.
- Rockafellar, R. T. *Convex Analysis*, volume 28. Princeton University Press, 1997.
- Rubner, Y., Tomasi, C., and Guibas, L. J. The earth mover’s distance as a metric for image retrieval. *International journal of computer vision*, 40(2):99–121, 2000.
- Schmitzer, B. Stabilized sparse scaling algorithms for entropy regularized transport problems. *SIAM Journal on Scientific Computing*, 41(3):A1443–A1481, 2019.
- Schrieber, J., Schuhmacher, D., and Gottschlich, C. DOTmark—a benchmark for discrete optimal transport. *IEEE Access*, 5:271–282, 2016.
- Shen, Z., Feydy, J., Liu, P., Curiale, A. H., San Jose Estepar, R., San Jose Estepar, R., and Niethammer, M. Accurate point cloud registration with robust optimal transport. *Advances in Neural Information Processing Systems*, 34: 5373–5389, 2021.
- Solodov, M. V. and Svaiter, B. F. An inexact hybrid generalized proximal point algorithm and some new results on the theory of Bregman functions. *Mathematics of Operations Research*, 25(2):214–230, 2000.
- Solomon, J., Rustamov, R., Guibas, L., and Butscher, A. Earth mover’s distances on discrete surfaces. *ACM Transactions on Graphics (ToG)*, 33(4):1–12, 2014.
- Tang, X., Shavlovsky, M., Rahmanian, H., Tardini, E., Thekumparampil, K. K., Xiao, T., and Ying, L. Accelerating Sinkhorn algorithm with sparse Newton iterations. In *The Twelfth International Conference on Learning Representations.*, 2024.

- Tang, Z. and Qiu, Y. Safe and sparse Newton method for entropic-regularized optimal transport. *Advances in Neural Information Processing Systems*, 37:129914–129943, 2024.
- Wang, C. and Qiu, Y. The sparse-plus-low-rank quasi-Newton method for entropic-regularized optimal transport. In *Forty-second International Conference on Machine Learning*, 2025.
- Wu, D., Liang, L., and Yang, H. PINS: Proximal iterations with sparse newton and sinkhorn for optimal transport. *arXiv preprint arXiv:2502.03749*, 2025.
- Xiao, H., Rasul, K., and Vollgraf, R. Fashion-MNIST: a novel image dataset for benchmarking machine learning algorithms. *arXiv preprint arXiv:1708.07747*, 2017.
- Xie, Y., Wang, X., Wang, R., and Zha, H. A fast proximal point method for computing exact wasserstein distance. In *Uncertainty in artificial intelligence*, pp. 433–453. PMLR, 2020.
- Yang, L. and Toh, K.-C. Bregman proximal point algorithm revisited: A new inexact version and its inertial variant. *SIAM Journal on Optimization*, 32(3):1523–1554, 2022.
- Zhang, G., Gu, Z., Yuan, Y., and Sun, D. HOT: An efficient halpern accelerating algorithm for optimal transport problems. *IEEE Transactions on Pattern Analysis and Machine Intelligence*, 47(8):6703–6714, 2025.

A. Converting a matrix to a transportation plan

Given a general non-negative matrix $X \in \mathbb{R}^{m \times n}$, the authors in (Altschuler et al., 2017) put forward a simple algorithm that returns a transportation plan $\hat{X} \in \mathbb{R}^{m \times n}$ satisfying $\hat{X}\mathbf{1}_n = \mathbf{a}$ and $\hat{X}^\top \mathbf{1}_m = \mathbf{b}$, where $\mathbf{1}_m^\top \mathbf{a} = \mathbf{1}_n^\top \mathbf{b} = 1$. The algorithm is shown below as Algorithm 3.

Algorithm 3 Converting a matrix X to a feasible transportation plan (Altschuler et al., 2017)

```

1: Input:  $X, \mathbf{a}, \mathbf{b}$ .
2: for  $i = 1, \dots, m$  do
3:    $z_i \leftarrow \min \left\{ \frac{a_i}{\sum_{j=1}^n X_{ij}}, 1 \right\}$ .
4: end for
5: Compute  $F = \text{diag}(z) X$ . % row sum is no greater than  $a_i$ 
6: for  $j = 1, \dots, n$  do
7:    $y_j \leftarrow \min \left\{ \frac{b_j}{\sum_{i=1}^m X_{ij}}, 1 \right\}$ .
8: end for
9: Update  $F \leftarrow F \text{diag}(y)$ . % column sum is no greater than  $b_i$ 
10: Compute  $\mathbf{e}_r \leftarrow \mathbf{a} - F\mathbf{1}_n$  and  $\mathbf{e}_c \leftarrow \mathbf{b} - F^\top \mathbf{1}_m$ .
11: Compute  $\hat{X} \leftarrow F + \mathbf{e}_r \mathbf{e}_c^\top / \|\mathbf{e}_r\|_1$ .
12: Output:  $\hat{X}$ .
```

B. Proofs of Theoretical Results

B.1. Proof of Lemma 3.1

Proof. Let (γ', ζ') be the solution to the two-dual problem (4). Note that the objective function in the semi-dual problem (6) can be rewritten as $\mathcal{L}^k(\gamma) = \min_{\zeta \in \mathbb{R}^m} Z^k(\gamma, \zeta) + C$, where C is a constant. Therefore, for any $\gamma \in \mathbb{R}^n$,

$$\mathcal{L}^k(\gamma) = \min_{\zeta \in \mathbb{R}^m} Z^k(\gamma, \zeta) + C \geq \min_{\gamma \in \mathbb{R}^n, \zeta \in \mathbb{R}^m} Z^k(\gamma, \zeta) + C = Z^k(\gamma', \zeta') + C.$$

On the other hand,

$$\mathcal{L}^k(\gamma') = \min_{\zeta \in \mathbb{R}^m} Z^k(\gamma', \zeta) + C \leq Z^k(\gamma', \zeta') + C.$$

Combining these two inequalities, we know

$$\mathcal{L}^k(\gamma') \leq Z^k(\gamma', \zeta') + C \leq \mathcal{L}^k(\gamma), \quad \forall \gamma \in \mathbb{R}^n.$$

Therefore, γ' is a solution to the problem (6). □

B.2. Proof of Theorem 3.2

Proof. For simplicity, let $W = P_\rho^\top \text{diag}(\mathbf{a}) P_\rho$. The matrix H_ρ is obviously symmetric. For arbitrary $\mathbf{z} \in \mathbb{R}^n$, we know

$$\mathbf{z}^\top H_\rho \mathbf{z} = \mathbf{z}^\top (\text{diag}(W\mathbf{1}_n) - W) \mathbf{z} / \eta = \frac{1}{2\eta} \sum_j \sum_k W_{jk} (z_j - z_k)^2 \geq 0, \quad (11)$$

Hence, H_ρ is positive semidefinite. Furthermore, by construction, there exists an i^* such that $(P_\rho)_{i^*j} > 0$ for $\forall j$, then $W_{jk} > 0$ for $\forall j, k$ and the above inequality (11) holds with equality for $z_j = z_k$ for $\forall j, k$. □

B.3. Proof of Theorem 3.3

Lemma B.1. For any $\mathbf{x} \in \mathbf{1}_n^\perp$, we have

$$\sum_j \sum_k (x_j - x_k)^2 = 2n \|\mathbf{x}\|^2. \quad (12)$$

Proof. Expanding the square within the summation, we have

$$\begin{aligned} \sum_j \sum_k (x_j - x_k)^2 &= \sum_j \sum_k (x_j^2 + x_k^2) - 2 \sum_j \sum_k x_j x_k \\ &= 2n \sum_j x_j^2 - 2 \left(\sum_j x_j \right)^2 = 2n \|\mathbf{x}\|^2. \end{aligned}$$

This completes the proof. \square

Now we are ready to prove Theorem 3.3.

Proof. Based on the construction of H_ρ , we know

$$W_{jk} = \sum_{i=1}^n a_i [P_\rho]_{ij} [P_\rho]_{ik} \geq a_{i^*} [P_\rho]_{i^*j} [P_\rho]_{i^*k} \geq a_{i^*} p^2.$$

Therefore, for any $\mathbf{z} \in \mathbf{1}_n^\perp$ with $\|\mathbf{z}\|^2 = 1$, we have

$$\mathbf{z}^\top H_\rho \mathbf{z} = \frac{1}{2\eta} \sum_j \sum_k W_{jk} (z_j - z_k)^2 \geq \frac{a_{i^*} p^2}{2\eta} \sum_j \sum_k (z_j - z_k)^2 = \frac{na_{i^*} p^2}{\eta}, \quad (13)$$

where the first equation follows from Theorem 3.2 and the final equation follows from Lemma B.1.

We consider the off-diagonal comments of W . Since $[P_\rho]_{ij} + \sum_{k \neq j} [P_\rho]_{ik} = 1$, we have

$$\sum_{k \neq j} W_{jk} = \sum_{k \neq j} \sum_{i=1}^n a_i [P_\rho]_{ij} [P_\rho]_{ik} = \sum_{i=1}^n a_i [P_\rho]_{ij} (1 - [P_\rho]_{ij}) \leq \sum_{i=1}^n \frac{a_i}{4} = \frac{1}{4}.$$

Note that the eigenvector \mathbf{v} corresponding to $\lambda(H_\rho) \neq 0$ satisfies $\mathbf{1}_n^\top \mathbf{v} = 0$, so $\mathbf{v} \in \mathbf{1}_n^\perp$. For any $\mathbf{z} \in \mathbb{R}^n$ with $\|\mathbf{z}\|^2 = 1$,

$$\mathbf{z}^\top H_\rho \mathbf{z} = \frac{1}{2\eta} \sum_j \sum_k W_{jk} (z_j - z_k)^2 \leq \frac{1}{\eta} \sum_j \sum_{k \neq j} W_{jk} (z_j^2 + z_k^2) = \frac{2}{\eta} \sum_j z_j^2 \sum_{k \neq j} W_{jk} \leq \frac{1}{2\eta}. \quad (14)$$

This completes the proof. \square

B.4. Proof of Theorem 3.4

We first present the approximation error of $E_P := P - P_\rho$, where P_ρ is construct via Algorithm 1.

Lemma B.2. *Let P and P_ρ constructed by Algorithm 1 for any $\rho \geq 0$, then*

$$\|E_P\|_\infty \leq 2n\rho, \quad \|E_P\|_1 \leq 2mn\rho, \quad \text{and} \quad \|E_P\| \leq 2\sqrt{mn}\rho.$$

Proof. To begin with, denote $K_i = \{j : P_{ij} < \rho\}$ and $J_i = \{j : P_{ij} \geq \rho\}$. Write $P_{i\cdot} = Q_{i\cdot} + S_{i\cdot}$ with

$$Q_{ij} = \begin{cases} P_{ij}, & j \in J_i \\ 0, & j \in K_i \end{cases}, \quad S_{ij} = \begin{cases} 0, & j \in J_i \\ P_{ij}, & j \in K_i \end{cases},$$

then $\sum_{j \in J_i} Q_{ij} = 1 - \sum_{j \in K_i} P_{ij} := 1 - r_i$ and $\sum_{j \in K_i} S_{ij} = r_i \leq n\rho$. Hence,

$$\|P_{i\cdot} - [P_\rho]_{i\cdot}\|_1 = \sum_{j \in J_i} \left| Q_{ij} - \frac{Q_{ij}}{1 - r_i} \right| + \sum_{j \in K_i} |S_{ij} - 0| = \left(\frac{1}{1 - r_i} - 1 \right) \sum_{j \in J_i} Q_{ij} + \sum_{j \in K_i} S_{ij} = 2r_i \leq 2n\rho.$$

Therefore, we obtain $\|E_P\|_\infty \leq 2n\rho$ and $\|E_P\|_1 \leq 2mn\rho$. In addition, $\|E_P\| \leq \sqrt{\|E_P\|_1 \|E_P\|_\infty} \leq 2\sqrt{mn}\rho$. \square

Now we show the approximation error between H and sparsified H_ρ .

Proof. To begin with, observe

$$H - H_\rho = \frac{1}{\eta} \left(\underbrace{\text{diag}(P^\top \mathbf{a} - P_\rho^\top \mathbf{a})}_{=:D_1} - \left(\underbrace{P^\top \text{diag}(\mathbf{a}) E_P}_{=:D_2} + \underbrace{(E_P)^\top \text{diag}(\mathbf{a}) P_\rho}_{D_3} \right) \right).$$

For D_1 , note that

$$\|D_1\| = \|\text{diag}((E_P)^\top \mathbf{a})\| = \|E_P^\top \mathbf{a}\|_\infty \leq \|\mathbf{a}\|_\infty \|E_P\|_1 \stackrel{\text{Lemma B.2}}{\leq} 2\rho mn \|\mathbf{a}\|_\infty.$$

For D_2 and D_3 , we have

$$\|D_2\| \leq \|P\| \|\mathbf{a}\|_\infty \|E_P\|, \quad \|D_3\| \leq \|E_P\| \|\mathbf{a}\|_\infty \|P_\rho\|.$$

In addition, since P_ρ satisfies $\|P_\rho\|_\infty = 1$ and $\|P_\rho\|_1 \leq m$ for any $\rho \geq 0$, we have $\|P_\rho\| \leq \sqrt{m}$. Hence

$$\|D_2\| + \|D_3\| \leq 2\sqrt{m} \|\mathbf{a}\|_\infty \|E_P\| \stackrel{\text{Lemma B.2}}{\leq} 4\rho mn \|\mathbf{a}\|_\infty.$$

Combining the two parts,

$$\|H - H_\rho\| \leq \frac{1}{\eta} (\|D_1\| + \|D_2\| + \|D_3\|) \leq \frac{6mn \|\mathbf{a}\|_\infty}{\eta} \rho.$$

□

B.5. Proof of Lemma 4.1

Proof. In the Newton stage, recall that the gradient satisfies $\mathbf{1}_n^\top \mathbf{g}^{k,v} = 0$ and the regularized Newton system is given by: $(H_\rho^{k,v} + \|\mathbf{g}^{k,v}\|I) \Delta \gamma^{k,v} = \mathbf{g}^{k,v}$. Multiplying both sides of the Newton system by $\mathbf{1}_n^\top$ from the left yields

$$\mathbf{1}_n^\top H_\rho^{k,v} \Delta \gamma^{k,v} + \|\mathbf{g}^{k,v}\| \mathbf{1}_n^\top \Delta \gamma^{k,v} = 0.$$

From Theorem 3.2, the sparsified Hessian satisfies $H_\rho^{k,v} \mathbf{1}_n = 0$. Due to the symmetry of $H_\rho^{k,v}$, we also have $\mathbf{1}_n^\top H_\rho^{k,v} = 0$. Consequently, the first term vanishes, leaving $\mathbf{1}_n^\top \Delta \gamma^{k,v} = 0$ if $\|\mathbf{g}^{k,v}\| \neq 0$. This ensures that the update maintains $\mathbf{1}_n^\top \gamma^{k,v+1} = 0$. □

B.6. Proof of Theorem 4.2

In the following analysis, we fix the outer iteration k . We first present the following lemmas.

Lemma B.3. *The set $S^{k,0}(\gamma) := \{\gamma : \mathcal{L}^k(\gamma) \leq \mathcal{L}^k(\gamma^{k,0})\}$ is bounded, closed, and convex, $\mathcal{L}^k(\gamma)$ is bounded below.*

Proof. First, it is easy to see that $\mathcal{L}^k(\gamma)$ is continuously differentiable and strictly convex, so $S_c^k := \{\gamma : \mathcal{L}^k(\gamma) \leq c\}$ is closed and convex.

Let $\gamma^{k,*}$ be an optimal solution to problem (6) and $\zeta^{k,*} := \zeta(\gamma)$ as defined in (5), then

$$Z^k(\gamma^{k,*}, \zeta^{k,*}) = \min_{\zeta \in \mathbb{R}^m} Z^k(\gamma^{k,*}, \zeta) = \mathcal{L}^k(\gamma^{k,*}) - C = \min_{\gamma \in \mathbb{R}^n} \mathcal{L}^k(\gamma) - C = \min_{\gamma \in \mathbb{R}^n, \zeta \in \mathbb{R}^m} Z^k(\gamma, \zeta),$$

where C is a constant. Therefore, $(\gamma^{k,*}, \zeta^{k,*})$ is an optimal solution to problem (4). By Lemma 1 in (Dvurechensky et al., 2018), we obtain

$$\max_j \gamma_j^{k,*} - \min_j \gamma_j^{k,*} \leq R,$$

where $R = \|C\|_\infty / \eta - \log(\min_{i,j} \{a_i, b_j\})$. It follows that $\|\gamma^{k,*}\| < \infty$ and then clearly $\mathcal{L}^{k,*} := \mathcal{L}^k(\gamma^{k,*}) > -\infty$. Obviously, $S_{\mathcal{L}^{k,*}}^k$ is non-empty and bounded, so $S^{k,0}(\gamma)$ is bounded by Corollary 8.7.1 in (Rockafellar, 1997). □

Lemma B.4. *Let $H_\rho^k(\gamma)$ be the matrix output by Algorithm 1, then for $\rho \geq 0$, there exist a constant $\underline{C}_k > 0$ such that $\lambda_{\min}(H_\rho^k(\gamma)|_{\mathbf{1}_n^\perp}) \geq \underline{C}_k$ for all $\gamma \in S^{k,0}(\gamma)$.*

Proof. By the boundedness of $S^{k,0}(\gamma)$, each element of $P^k(\gamma)$ as defined in (7) is bounded below from zero over $S^{k,0}(\gamma)$. Recall the lower bound of $\lambda_{\min}(H_\rho^k(\gamma)|_{\mathbf{1}_n^\perp})$ established in Theorem 3.3, we conclude that there exists a constant $\underline{C}_k > 0$ such that $\lambda_{\min}(H_\rho^k(\gamma)|_{\mathbf{1}_n^\perp}) \geq \underline{C}_k$ holds for any $\rho \geq 0$ and all $\gamma \in S^{k,0}(\gamma)$. \square

As shown in Lemma 4.1, the convergence analysis can be safely restricted to $\mathbf{1}_n^\perp$, we then denote $\lambda_{\min}(H_\rho^{k,v}|_{\mathbf{1}_n^\perp})$ by $\lambda_{\min}(H_\rho^{k,v})$ in the subsequent analysis for notational simplicity. We then show that $\Delta\gamma^{k,v}$ is a descent direction and provide the minimum stepsize.

Lemma B.5. *In the outer k iteration, let $\{\gamma^{k,v}\}_v$ be the sequence generated by Algorithm 2 satisfying $\mathbf{1}_n^\top \gamma^{k,0} = 0$, $\Delta\gamma^{k,v}$ be a direction for \mathcal{L}^k and we choose $t^{k,v}$ as stepsize by Armijo backtracking, then*

(i) $\Delta\gamma^{k,v}$ is a descent direction for \mathcal{L}^k ;

(ii) the backtracking terminates finitely with a step size $t^{k,v}$ bounded below by

$$t^{k,v} \geq \bar{t}_{\min}^{k,v} := \min \left\{ 1, \beta \frac{4\eta(1-\sigma)[\lambda_{\min}(H_\rho^{k,v})]^2}{1/2\eta + 2} \right\} > 0, \quad (15)$$

where $\beta \in (0, 1)$ is the backtracking contraction factor and $\sigma \in (0, 1)$ is the Armijo parameter.

Proof. (i) To begin with, it is easy to see that

$$(\mathbf{g}^{k,v})^\top \Delta\gamma^{k,v} = -(\mathbf{g}^{k,v})^\top (H_\rho^{k,v} + \|\mathbf{g}^{k,v}\|I)^{-1} \mathbf{g}^{k,v} < 0,$$

where $\mathbf{g}^{k,v}$ is the gradient of \mathcal{L}^k on $\gamma^{k,v}$ and the inequality due to Theorem 3.2. Therefore, $\Delta\gamma^{k,v}$ is a descent direction.

(ii) Since $\lambda_{\max}(H_\rho) \leq 1/(2\eta)$ for any $\rho \geq 0$ from Theorem 3.3, $\mathbf{g}^{k,v}$ is $1/(2\eta)$ -Lipschitz continuous, and the standard quadratic upper bound yields

$$\mathcal{L}^k(\gamma^{k,v} + t\Delta\gamma^{k,v}) \leq \mathcal{L}^k(\gamma^{k,v}) + t(\mathbf{g}^{k,v})^\top \Delta\gamma^{k,v} + \frac{1}{4\eta} t^2 \|\Delta\gamma^{k,v}\|^2.$$

Hence any t with

$$0 < t \leq \bar{t}^{k,v} := \frac{4\eta(1-\sigma)(-\mathbf{g}^{k,v})^\top \Delta\gamma^{k,v}}{\|\Delta\gamma^{k,v}\|^2}$$

satisfies the Armijo inequality $\mathcal{L}^k(\gamma^{k,v} + t\Delta\gamma^{k,v}) \leq \mathcal{L}^k(\gamma^{k,v}) + \sigma t(\mathbf{g}^{k,v})^\top \Delta\gamma^{k,v}$.

We now provide a lower bound for $\bar{t}^{k,v}$. First, note that

$$\begin{aligned} -(\mathbf{g}^{k,v})^\top \Delta\gamma^{k,v} &= (\mathbf{g}^{k,v})^\top (H_\rho^{k,v} + \|\mathbf{g}^{k,v}\|I)^{-1} \mathbf{g}^{k,v} \geq \frac{1}{\lambda_{\max}(H_\rho^{k,v}) + \|\mathbf{g}^{k,v}\|} \|\mathbf{g}^{k,v}\|^2, \\ \|\Delta\gamma^{k,v}\| &= (H_\rho^{k,v} + \|\mathbf{g}^{k,v}\|I)^{-1} \mathbf{g}^{k,v} \leq \frac{1}{\lambda_{\min}(H_\rho^{k,v}) + \|\mathbf{g}^{k,v}\|} \|\mathbf{g}^{k,v}\| \leq \frac{1}{\lambda_{\min}(H_\rho^{k,v})} \|\mathbf{g}^{k,v}\|. \end{aligned}$$

Combining these,

$$\bar{t}^{k,v} \geq \frac{4\eta(1-\sigma)[\lambda_{\min}(H_\rho^{k,v})]^2}{\lambda_{\max}(H_\rho^{k,v}) + \|\mathbf{g}^{k,v}\|} \geq \frac{4\eta(1-\sigma)[\lambda_{\min}(H_\rho^{k,v})]^2}{\lambda_{\max}(H_\rho^{k,v}) + 2},$$

where the final inequality holds since $\|\mathbf{g}^{k,v}\| \leq \|(P^k(\gamma^{k,v}))^\top \mathbf{a}\| + \|\mathbf{b}\| \leq 2$. Backtracking with ratio β accepts some $t^{k,v} \geq \beta \bar{t}^{k,v}$ and using the bound $\lambda_{\max}(H_\rho^{k,v}) \leq 1/(2\eta)$ and $\lambda_{\min}(H_\rho^{k,v}) > 0$ in Theorem 3.3, yields (15). \square

Next, we provide the proof of Theorem 4.2.

Proof. (i) From Lemma B.5, we know

$$-(\mathbf{g}^{k,v})^\top \Delta \gamma^{k,v} \geq \frac{1}{\lambda_{\max}(H^{k,v}) + \|\mathbf{g}^{k,v}\|} \|\mathbf{g}^{k,v}\|^2 \geq \frac{1}{1/(2\eta) + 2} \|\mathbf{g}^{k,v}\|^2,$$

since $\|\mathbf{g}^{k,v}\| \leq 2$. It further yields

$$\mathcal{L}^k(\gamma^{k,v+1}) - \mathcal{L}^k(\gamma^{k,v}) \leq -\sigma t_{\min}^{k,v} \cdot \frac{1}{1/(2\eta) + 2} \|\mathbf{g}^{k,v}\|^2, \quad (16)$$

where $t_{\min}^{k,v}$ is defined in Lemma B.5. Thus $\{\mathcal{L}^k(\gamma^{k,v})\}_v$ is monotonically decreasing and $\gamma^{k,v} \in S^k(\gamma)$ for all v . By Lemma B.4, we know $\lambda_{\min}(H_\rho^{k,v}) \geq \underline{C}_k > 0$ for all v and $\rho \geq 0$ over $S^{k,0}(\gamma)$. This allows us to define a uniform lower bound for the step size:

$$t_{\min}^{k,v} \geq t_{\min}^k := \min \left\{ 1, \beta \frac{4\eta(1-\sigma)\underline{C}_k^2}{1/2\eta + 2} \right\}.$$

In addition, since \mathcal{L}^k is bounded below by Lemma B.3, the telescoping sum of (16) implies $\sum_v \|\mathbf{g}^{k,v}\|^2 < \infty$. Therefore, we conclude that $\|\mathbf{g}^{k,v}\| \rightarrow 0$ as $v \rightarrow \infty$.

(ii) By the definition of $\gamma^{k,*}$, we know $g^k(\gamma^{k,*}) \in \text{span}\{\mathbf{1}_n\}$, where $g^k(\gamma)$ is defined in (8). On the other hand, it is easy to check that for all $\gamma \in \mathbb{R}^n$, $\mathbf{1}_n^\top g^k(\gamma) = 0$. Combining the two relations implies $g^k(\gamma^{k,*}) = \mathbf{0}_n$.

Over $S^{k,0}(\gamma)$ and $\mathbf{1}_n^\perp$, since \mathcal{L}^k is \underline{C}_k -strongly convex, the solution of \mathcal{L}^k is unique and

$$\|\mathbf{g}^{k,v}\| = \|\mathbf{g}^{k,v} - g^k(\gamma^{k,*})\| \geq \underline{C}_k \|\gamma^{k,v} - \gamma^{k,*}\|$$

by Theorem 2.1.10 in (Nesterov et al., 2018). Since $\|\mathbf{g}^{k,v}\| \rightarrow 0$, it follows that $\gamma^{k,v} \rightarrow \gamma^{k,*}$ as $v \rightarrow \infty$, where $\gamma^{k,*}$ satisfies $\mathbf{1}_n^\top \gamma^{k,*} = 0$. \square

B.7. Proof of Theorem 4.3

Proof. The following proof is motivated by (Tang & Qiu, 2024). By Theorem 3.3 and Lipschitz continuity of $H^{k,v}$, we have

$$\begin{aligned} \|\mathbf{g}^{k,v}\| &\leq 1/(2\eta) \|\gamma^{k,v} - \gamma^{k,*}\|, \\ \|\mathbf{g}^{k,v} - g^k(\gamma^{k,*}) - H^{k,v}(\gamma^{k,v} - \gamma^{k,*})\| &\leq \frac{L_H}{2} \|\gamma^{k,v} - \gamma^{k,*}\|^2. \end{aligned}$$

In addition, denote $B_\rho^{k,v} := H_\rho^{k,v} + \|\mathbf{g}^{k,v}\| I$, we have

$$\|H^{k,v} - B_\rho^{k,v}\| \leq \|H^{k,v} - H_\rho^{k,v}\| + \|\mathbf{g}^{k,v}\| \leq (6\|\mathbf{a}\|_\infty + 1) \|\mathbf{g}^{k,v}\| \leq \frac{6\|\mathbf{a}\|_\infty + 1}{2\eta} \|\gamma^{k,v} - \gamma^{k,*}\|,$$

where the second inequality holds due to Theorem 3.4.

In addition, since $\gamma^{k,v} \in S^{k,0}(\gamma)$, we have

$$\|(B_\rho^{k,v})^{-1}\| = (\lambda_{\min}(B_\rho^{k,v}))^{-1} \leq (\lambda_{\min}(H_\rho^{k,v}))^{-1} \leq \underline{C}_k^{-1},$$

where $\underline{C}_k > 0$ is defined in Lemma B.4. As a result,

$$\begin{aligned} \|\gamma^{k,v+1} - \gamma^{k,*}\| &= \|\gamma^{k,v} + \Delta \gamma^{k,v} - \gamma^{k,*}\| = \|\gamma^{k,v} - \gamma^{k,*} - (B_\rho^{k,v})^{-1} \mathbf{g}^{k,v}\| \\ &= \|(B_\rho^{k,v})^{-1} (B_\rho^{k,v} (\gamma^{k,v} - \gamma^{k,*}) - \mathbf{g}^{k,v})\| \\ &\leq \|(B_\rho^{k,v})^{-1}\| \cdot \|\mathbf{g}^{k,v} - g^k(\gamma^{k,*}) - H^{k,v}(\gamma^{k,v} - \gamma^{k,*}) + (H^{k,v} - B_\rho^{k,v})(\gamma^{k,v} - \gamma^{k,*})\| \\ &\leq \underline{C}_k^{-1} (\|\mathbf{g}^{k,v} - g^k(\gamma^{k,*}) - H^{k,v}(\gamma^{k,v} - \gamma^{k,*})\| + \|(H^{k,v} - B_\rho^{k,v})(\gamma^{k,v} - \gamma^{k,*})\|) \\ &\leq \underline{C}_k^{-1} \left(\frac{1}{2} L_H \|\gamma^{k,v} - \gamma^{k,*}\|^2 + \frac{6\|\mathbf{a}\|_\infty + 1}{2\eta} \|\gamma^{k,v} - \gamma^{k,*}\|^2 \right) \\ &= \underline{C}_k^{-1} \left(\frac{1}{2} L_H + \frac{6\|\mathbf{a}\|_\infty + 1}{2\eta} \right) \|\gamma^{k,v} - \gamma^{k,*}\|^2. \end{aligned}$$

\square

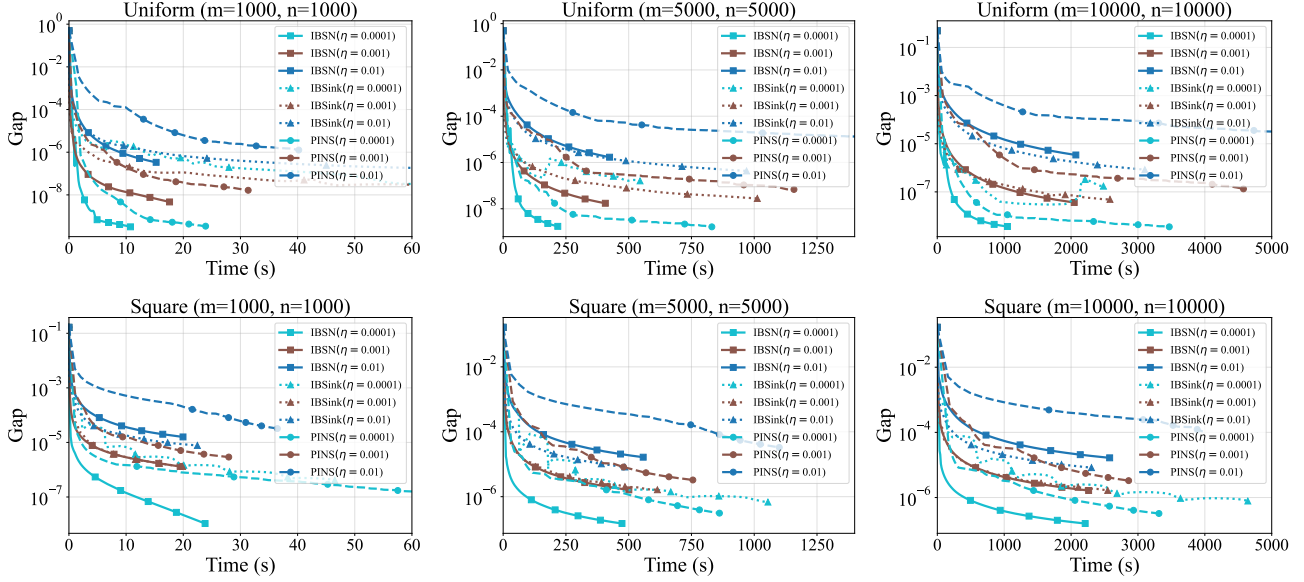


Figure 4. Impact of the regularization parameter η on IBSN, IBSink and PINS on synthetic data. Top: Uniform setting. Bottom: Square setting.

C. Additional Experiment Details

C.1. Derivation of relative KKT residual Δ_{kkt}

One can show that the dual problem of (1) is

$$\max_{\gamma \in \mathbb{R}^n, \zeta \in \mathbb{R}^m} \mathbf{a}^\top \zeta + \mathbf{b}^\top \gamma \quad \text{s.t.} \quad U(\gamma, \zeta) := C - \zeta \mathbf{1}_n^\top - \mathbf{1}_m \gamma^\top \geq 0 \quad (17)$$

with KKT system

$$X \mathbf{1}_n = \mathbf{a}, \quad X^\top \mathbf{1}_m = \mathbf{b}, \quad \langle X, U(\gamma, \zeta) \rangle = 0, \quad X \geq 0, \quad U(\gamma, \zeta) \geq 0. \quad (18)$$

Based on (18), the relative KKT residual Δ_{kkt} is defined as:

$$\Delta_{\text{kkt}} := \max\{\Delta_p, \Delta_d, \Delta_c\}, \quad (19)$$

where $\Delta_p := \max\left\{\frac{\|X \mathbf{1}_n - \mathbf{a}\|}{1 + \|\mathbf{a}\|}, \frac{\|X^\top \mathbf{1}_m - \mathbf{b}\|}{1 + \|\mathbf{b}\|}, \frac{\|\min\{X, 0\}\|_F}{1 + \|X\|_F}\right\}$, $\Delta_d := \frac{\|\min\{U(\gamma, \zeta), 0\}\|_F}{1 + \|C\|_F}$, $\Delta_c := \frac{|\langle X, U(\gamma, \zeta) \rangle|}{1 + \|C\|_F}$, and $\|\cdot\|_F$ is the Frobenius norm of a matrix. Clearly, $\Delta_{\text{kkt}} = 0$ if and only if (X, γ, ζ) satisfies the KKT system (18), making Δ_{kkt} a natural measure of optimality. In our semi-dual formulation (6), we compute ζ via the *c-transform*: $\zeta_i = \min_{j \in [n]} (C_{ij} - \gamma_j)$ $\forall i \in [m]$.

C.2. Impact of the regularization parameter η

In this section, we investigate the effect of the regularization parameter η on the performance of the IBSN, PINS, and IBSink algorithms under the synthetic settings.

The results, shown in Figure 4, demonstrate that IBSN consistently outperforms PINS across all configurations, achieving faster convergence and smaller objective gaps for the same η . In addition, as η increases, both methods exhibit slower convergence, reflecting the effect of stronger regularization.

C.3. Impact of the sparsity in the Newton phase

To assess the effectiveness of the sparsity process introduced in the Newton phase, we compare the proposed IBSN algorithm with its non-sparse counterpart, denoted as IBN (IBSN without sparsity process during the Newton stage). Both methods are

Table 1. Performance comparison between IBSN and IBN (IBSN without sparsity process during the Newton stage).

Size $m = n = 1000$									
Synthetic: Uniform					Synthetic: Square				
Alg	NewtonIte	CGTime (s)	Time (s)	Gap	Alg	NewtonIte	CGTime (s)	Time (s)	Gap
IBN	177	28.38	33.47	3.18e-10	IBN	301	61.55	72.03	1.07e-08
IBSN	176	3.86	11.04	3.19e-10	IBSN	301	11.13	24.68	1.07e-08
Size $m = n = 5000$									
Synthetic: Uniform					Synthetic: Square				
Alg	NewtonIte	CGTime (s)	Time (s)	Gap	Alg	NewtonIte	CGTime (s)	Time (s)	Gap
IBN	174	497.19	659.57	1.70e-09	IBN	301	803.53	1101.43	1.49e-07
IBSN	174	9.69	219.22	1.70e-09	IBSN	301	74.37	457.10	1.49e-07
Size $m = n = 10000$									
Synthetic: Uniform					Synthetic: Square				
Alg	NewtonIte	CGTime (s)	Time (s)	Gap	Alg	NewtonIte	CGTime (s)	Time (s)	Gap
IBN	167	1688.99	2522.38	3.65e-09	IBN	300	2654.52	4303.08	1.59e-07
IBSN	170	16.82	921.60	3.63e-09	IBSN	300	267.15	2205.74	1.59e-07

Bold values indicate the most favorable results. The algorithm terminates when $\Delta_{\text{kkt}} < 10^{-11}$ or after 300 outer iterations. “NewtonIte”, “CGTime” and “Time” represent the total number of Newton iteration, total runtime for finding the Newton directions and total running time for the algorithm, respectively.

evaluated on the Uniform and Square synthetic cost settings with problem sizes $m = n \in \{1000, 5000, 10000\}$. The results are given in Table 1.

As observed from the table, introducing sparsity into the Hessian computation leads to a substantial reduction in the computational cost of solving the Newton systems, while achieving identical final gaps. In addition, the benefit of sparsity becomes more pronounced in finding a Newton direction as the problem size increases. We also observe that the total runtime advantage decreases for larger problems, this is primarily because other computational components, such as line search and the evaluation of the stopping criterion based on $D_\phi(\mathcal{P}_\Omega(X^{k+1}), X^{k+1})$, begin to dominate the overall cost. Nevertheless, the significant reduction in the time required for Newton direction computation clearly demonstrates the effectiveness of the proposed sparsity process in accelerating the Newton phase.

C.4. Impact of the semi-dual formulation on Newton direction computation

In this subsection, we investigate the impact of the semi-dual formulation on the efficiency of computing the Newton direction. To do this, we compare the proposed IBSN algorithm with three second-order methods, PINS, SSNS, and SPLR. The baselines use the standard dual formulation with two dual variables, while IBSN works in the semi-dual space. We also use a shared warm start: run the Sinkhorn algorithm until the gradient norm is below 10^{-3} , then switch to the Newton-type phase. This reduces sensitivity to initialization and makes the comparison focus on the Newton step. In addition, we also provide Sinkhorn algorithm as a reference.

Since PINS and IBSN are originally designed to solve the exact OT problem (which involves a sequence of subproblems), we adapted them for this specific experiment. In both frameworks, each subproblem can be regarded as an EOT problem with a modified cost matrix $C - \eta \log(X^k)$. To ensure they solve the exact same EOT problem as the other methods, we fix $X^k = \mathbf{1}_m \mathbf{1}_n^\top$ and limit the algorithms to solve the subproblem just once, rather than iteratively. This modification ensures that all algorithms are addressing the same single EOT problem with the original cost matrix C . We refer to these adapted versions as (E)PINS and (E)IBSN.

In the following experiments, we evaluate the impact of the semi-dual formulation across two distinct scenarios: (i) the balanced setting where $m = n$, and (ii) the unbalanced setting where $m > n$. The algorithm terminates when the gradient norm is less than 10^{-9} or attains its maximum number of iterations.

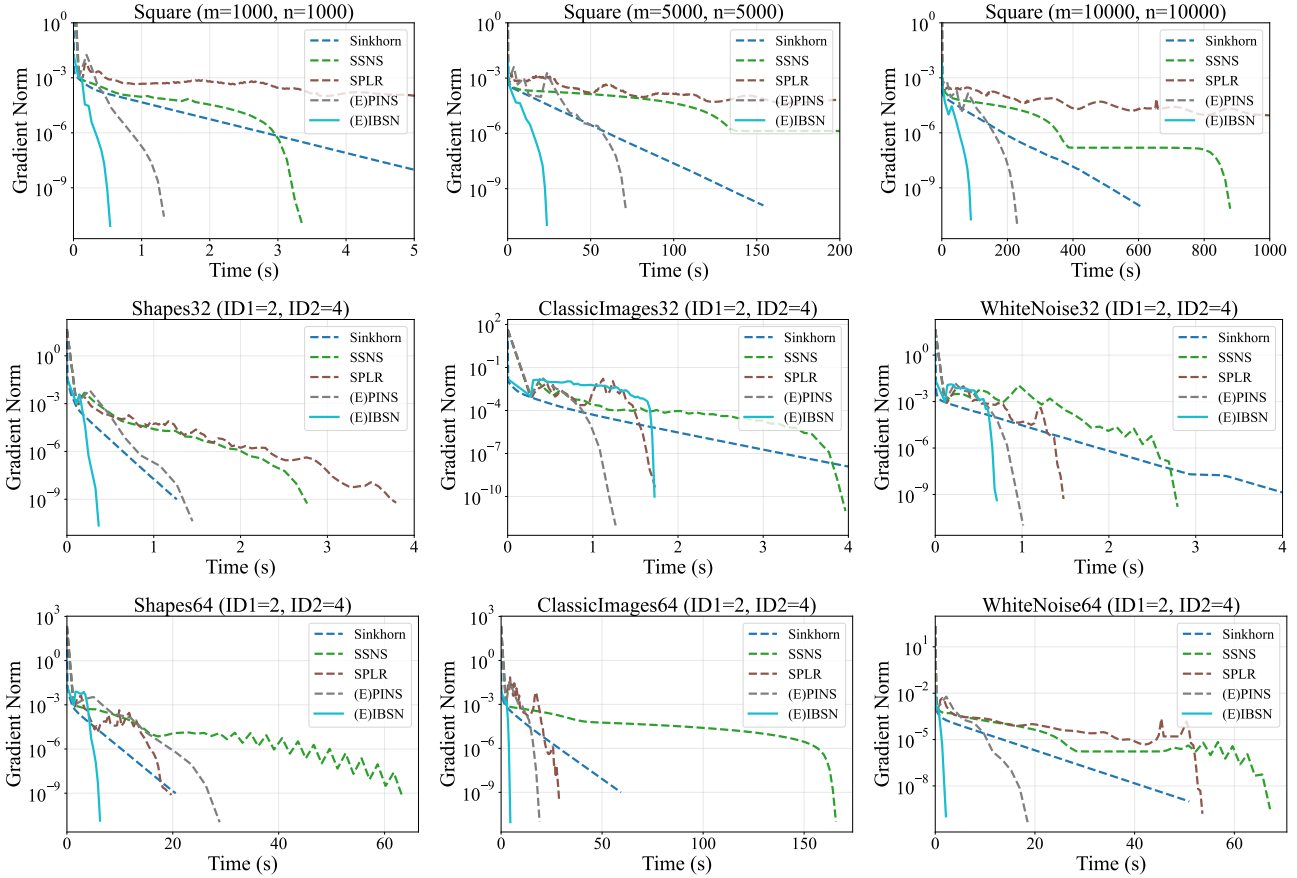


Figure 5. Performance of different algorithms on EOT problem (2). Top: Square setting. Middle: DOTmark with image size 32×32 . Bottom: DOTmark with image size 64×64 .

Performance on balanced $m = n$. We first evaluate performance using the synthetic Square setting and the real DOTmark dataset, with the regularization parameter fixed at $\eta = 10^{-4}$. As shown in Figure 5, our proposed algorithm (E)IBSN performs well in both synthetic and real data. In addition, second-order methods typically exhibit a faster convergence rate than Sinkhorn algorithm once they enter the Newton regime. Table 2 presents more details about the cost of the Newton step. Across all experimental settings, IBSN requires the fewest CG iterations to find the Newton direction—typically only about half as many iterations as the other second-order methods. This efficiency stems directly from our semi-dual formulation, which reduces the dimensionality of the dual space and simplifies the linear system significantly.

Performance on unbalanced $m > n$. Next, we investigate the performance of the algorithms in unbalanced settings where $m > n$. To do this, we conduct experiments on a spherical transport problem between supply and demand locations, inspired by Amos et al. (2023). The cost matrix $C \in \mathbb{R}^{m \times n}$ is given by the spherical distance, i.e., $C_{ij} = \arccos(\langle \mathbf{x}_i, \mathbf{y}_j \rangle)$, where $\mathbf{x}_i, \mathbf{y}_j \in \mathbb{S} := \{\mathbf{z} \in \mathbb{R}^3 : \|\mathbf{z}\| = 1\}$. For the data generation, the demand locations $\{\mathbf{x}_i\}_{i=1}^m$ from Earth’s population density data (Doxsey-Whitfield et al., 2015), while the supply locations $\{\mathbf{y}_j\}_{j=1}^n$ are sampled uniformly from Earth’s landmass. The marginal weights \mathbf{a} and \mathbf{b} are sampled independently from a uniform distribution on $(0, 1)$ and normalized such that $\mathbf{1}_m^\top \mathbf{a} = \mathbf{1}_n^\top \mathbf{b} = 1$. We set the regularization parameter to $\eta = 10^{-3}$.

Figure 6 demonstrates that (E)IBSN requires the fewest mean number of CG iterations to find a Newton direction and consistently outperforms among all algorithms as the source dimension m increases. This efficiency is attributed to our semi-dual formulation, which restricts the Hessian matrix to a low dimension regardless of the growth in the source dimension m .

Table 2. Performance of different algorithms in Newton direction computation under EOT problem (2).

Synthetic: Square									
	size $m = n = 1000$			size $m = n = 5000$			size $m = n = 10000$		
Alg	MeanCG	Ite	Time (s)	MeanCG	Ite	Time (s)	MeanCG	Ite	Time (s)
SSNS	305.8 (69)	34	3.36	712.4 (92)	116	373.37	749.4 (135)	61	879.52
SPLR	- (-)	-	20.44	- (-)	-	554.80	- (-)	-	2068.48
(E)PINS	292.8 (49)	14	1.33	418.0 (143)	22	71.24	425.5 (173)	17	229.77
(E)IBSN	163.6 (16)	11	0.54	290.4 (88)	13	23.64	241.2 (97)	13	88.63
Real: DOTmark (ID1 = 2, ID2 = 4) with size $m = n = 1024$									
	Shapes32			ClassicImages32			WhiteNoise32		
Alg	MeanCG	Ite	Time (s)	MeanCG	Ite	Time (s)	MeanCG	Ite	Time (s)
SSNS	1071.3 (383)	23	2.77	371.9 (89)	40	3.97	346.3 (129)	29	2.79
SPLR	694.9 (528)	80	3.79	210.3 (144)	50	1.74	233.3 (110)	47	1.48
(E)PINS	763.2 (251)	9	1.45	318.6 (67)	11	1.27	317.7 (76)	10	1.01
(E)IBSN	360.3 (79)	8	0.37	163.7 (27)	43	1.72	164.6 (34)	20	0.71
Real: DOTmark (ID1 = 2, ID2 = 4) with size $m = n = 4096$									
	Shapes64			ClassicImages64			WhiteNoise64		
Alg	MeanCG	Ite	Time (s)	MeanCG	Ite	Time (s)	MeanCG	Ite	Time (s)
SSNS	770.4 (190)	43	63.24	275.5 (99)	113	165.73	396.4 (87)	46	67.17
SPLR	509.4 (205)	46	19.73	151.0 (110)	71	28.75	219.8 (76)	123	53.60
(E)PINS	617.9 (206)	12	28.85	265.1 (57)	11	19.05	324.5 (78)	11	18.53
(E)IBSN	236.0 (113)	14	6.26	162.3 (27)	7	4.58	195.2 (25)	6	2.14

Bold values indicate the most favorable results. “MeanCG” denotes the mean number (standard error) of CG iterations in finding a Newton direction, and “Ite” denotes the total number of iterations. “-” indicates the algorithm attains its maximum number of iterations, and its gradient norm is larger than 10^{-9} .

C.5. More comparisons on EOT problem (2)

In this subsection, we extend our comparison to include the following methods, all implemented using the Python-OT (POT) package (Flamary et al., 2021; 2024):

- L2ROT: Solve the OT problem using ℓ_2 -regularization (Blondel et al., 2018).
- S2EOT: Solve the EOT problem using sparsity-constrained regularization (Liu et al., 2023) (sparsity is chosen as 2).
- LogSink: Solve the EOT problem using Sinkhorn-Knopp matrix scaling algorithm with the log stabilization (Schmitzer, 2019).
- GCG: Solve the OT problem using ℓ_2 and entropic regularization with the generalized conditional gradient algorithm (Courty et al., 2017b; Rakotomamonjy et al., 2015).

All regularization parameters are set to be 10^{-4} . Table 3 presents the results. Our proposed (E)IBSN algorithm consistently outperforms these baselines on both synthetic and real datasets, achieving significantly lower gradient norms in less computational time. These results demonstrate that (E)IBSN is a highly effective and robust solver for EOT problems (2).

D. Color transfer

Color transfer aims to modify the color distribution of a source image so that it matches the color palette of a target image, while preserving the structural content of the source. Specifically, by interpreting image colors as probability distributions in

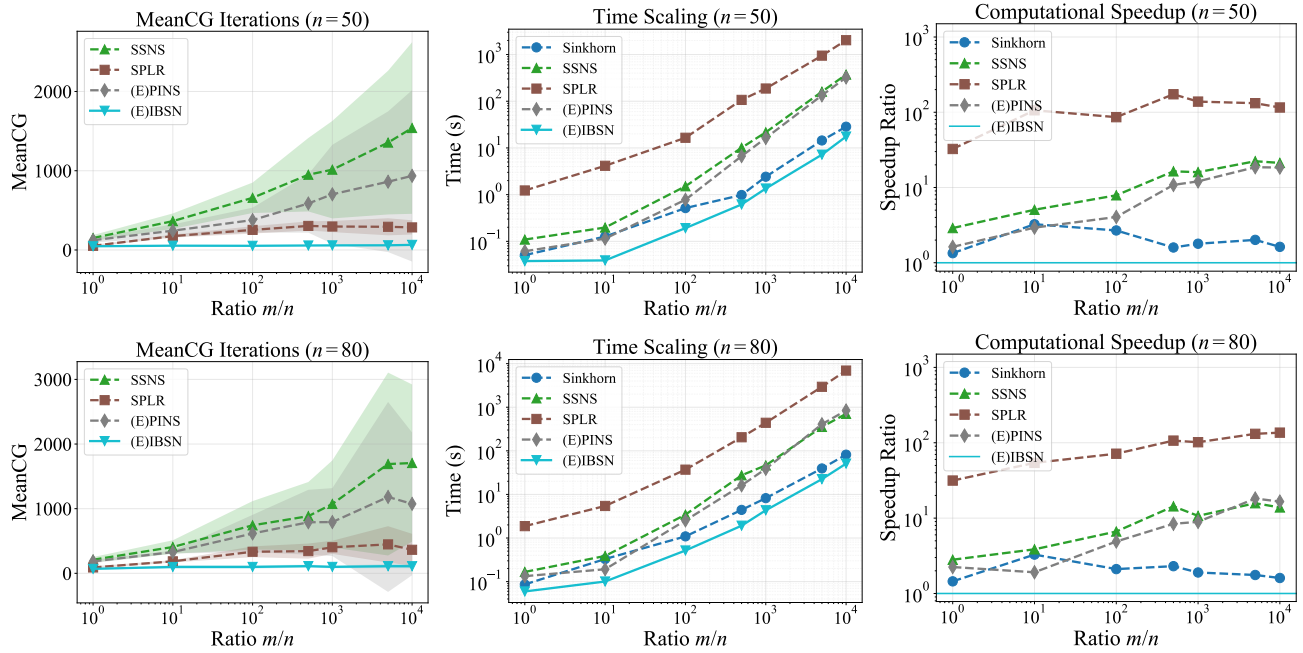


Figure 6. Scalability analysis on highly unbalanced spherical OT problems. The target dimension is fixed at $n = 50$ (top) and $n = 80$ (bottom). Left: Mean number of CG iterations required to compute a Newton direction, with shaded regions representing the standard error. Middle: Total running time in log-log scale. Right: Speedup ratio of (E)IBSN relative to other algorithms. A value of $c > 1$ indicates that (E)IBSN is c times faster than the competing algorithm.

a suitable color space, the optimal transport framework provides a method for transferring color characteristics between images.

Following the experimental protocol in (Zhang et al., 2025), we conduct the color transfer experiments in the CIE-Lab color space. We apply the K-means clustering algorithm with $K = 512$ to quantize the color space of each image, and use the resulting cluster centers and their normalized frequencies to construct the discrete color distributions. The proposed IBNS algorithm is then employed to compute the optimal transport plan between these two distributions, and the resulting mapping is used to transfer the target’s color style onto the source image. The results of color transfer for selected image pairs can be found in Figure 7.

Table 3. Comparison of different algorithms in POT package when solving EOT problem (2).

Synthetic: Square								
size $m = n = 1000$			size $m = n = 5000$			size $m = n = 10000$		
Alg	GradNorm	Time (s)	Alg	GradNorm	Time (s)	Alg	GradNorm	Time (s)
L2ROT	1.90e-02	3.79	L2ROT	1.13e-02	144.34	L2ROT	5.55e-03	548.38
S2EOT	2.61e-02	5.65	S2EOT	9.57e-03	209.74	S2EOT	5.88e-03	833.64
LogSink	5.14e-02	25.49	LogSink	2.31e-02	774.38	LogSink	1.63e-02	2530.27
GCG	1.37e-04	2.33	GCG	1.43e-04	64.16	GCG	3.75e-05	217.92
(E)IBSN	8.44e-12	0.55	(E)IBSN	1.08e-11	22.89	(E)IBSN	1.92e-11	90.91
Real: DOTmark (ID1 = 2, ID2 = 4) with size $m = n = 1024$								
Shapes32			ClassicImages32			WhiteNoise32		
Alg	GradNorm	Time (s)	Alg	GradNorm	Time (s)	Alg	GradNorm	Time (s)
L2ROT	8.18e-02	5.62	L2ROT	1.08e-01	4.89	L2ROT	4.27e-02	4.39
S2EOT	8.02e-01	14.34	S2EOT	2.62e-01	10.75	S2EOT	7.74e-02	9.99
LogSink	6.20e-02	28.92	LogSink	4.75e-02	27.41	LogSink	5.09e-02	27.04
GCG	4.56e-06	2.15	GCG	2.43e-04	2.20	GCG	1.89e-04	2.17
(E)IBSN	2.25e-11	0.37	(E)IBSN	9.72e-11	1.72	(E)IBSN	4.30e-10	0.71
Real: DOTmark (ID1 = 2, ID2 = 4) with size $m = n = 4096$								
Shapes64			ClassicImages64			WhiteNoise64		
Alg	GradNorm	Time (s)	Alg	GradNorm	Time (s)	Alg	GradNorm	Time (s)
L2ROT	2.85e-01	103.11	L2ROT	1.41e-01	85.52	L2ROT	1.80e-02	79.11
S2EOT	3.19e-01	276.25	S2EOT	8.48e-02	219.66	S2EOT	2.68e-02	199.39
LogSink	3.12e-02	439.69	LogSink	2.40e-02	440.81	LogSink	2.55e-02	435.39
GCG	4.03e-06	34.64	GCG	1.22e-04	41.49	GCG	4.09e-05	40.48
(E)IBSN	1.39e-11	6.26	(E)IBSN	9.19e-12	4.58	(E)IBSN	1.08e-10	2.14

Bold values indicate the most favorable results. The algorithm terminates when the gradient norm (GradNorm) is less than 10^{-9} or attains its maximum number of iterations.

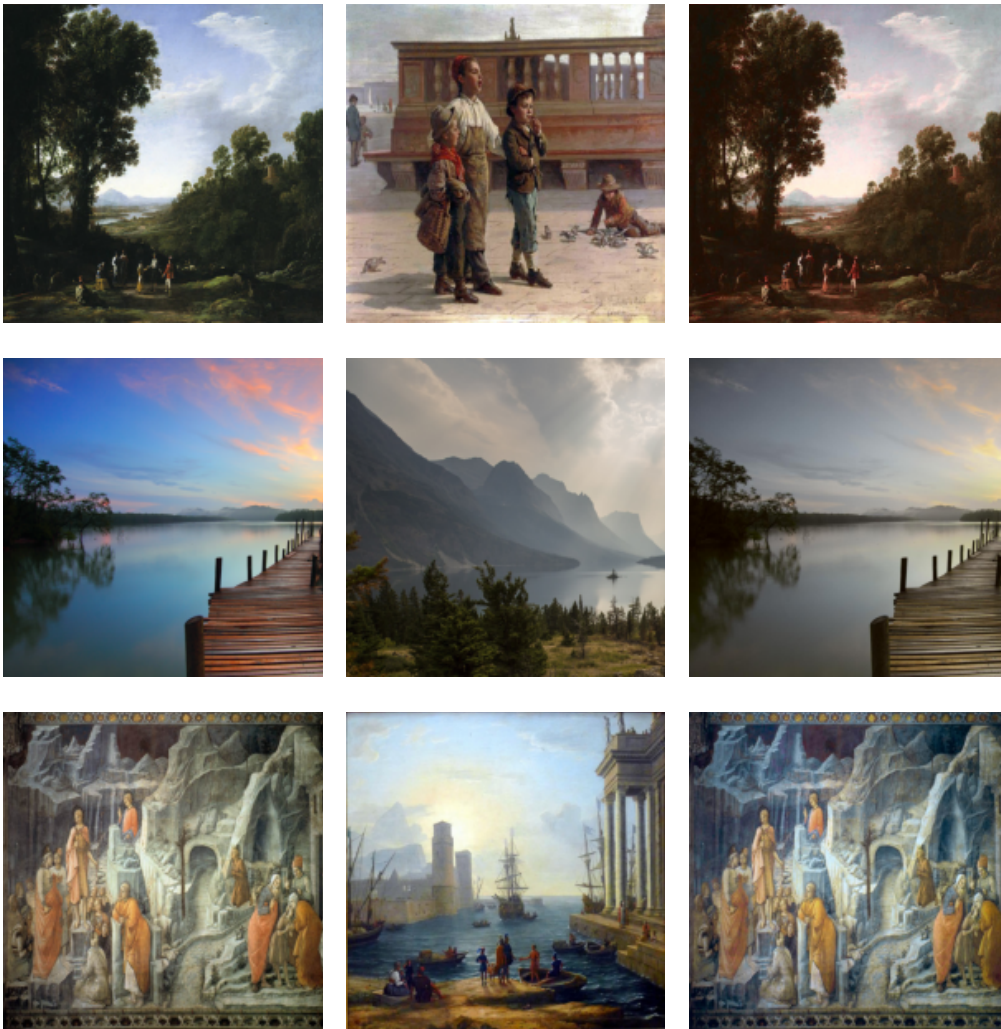


Figure 7. Color transfer results obtained using the IBSN algorithm. Each triplet shows the source image (left), the target image (middle), and the resulting image after applying color transfer (right).